ADVANCED FUNCTIONAL MATERIALS
www.afm-journal.de

# Photoswitching Conduction in Framework Materials

*Helmy Pacheco Hernandez, Stefan Hecht, Wolfgang Wenzel, Lars Heinke, and Mariana Kozlowska**

**Light is an attractive non-invasive stimulus that permits the activation and control of properties and functions in precise and tunable ways. It inspired scientists and engineers to develop different applications, including those based on conductivity, magnetism or reactivity, and to design light-responsive materials that can sense, adapt, and self-heal under illumination. Often, photoactive molecules that can reversibly undergo photoisomerization serve as the key component to achieve light-switching of functionalities in advanced materials for reconfigurable electronics or light-controlled information storage and processing. However, when used in bulk or solution, they face limitations such as aggregation or restricted isomerization. Their integration into frameworks materials overcomes these challenges, paving the way for new photoprogrammed materials. This review shows the potential of framework materials for light-switched conduction, focusing specifically on proton and electron conduction photoswitching. This work reviews the recent progress in state-of-the-art and explains the mechanisms driving the photoresponse, including the Grotthuss mechanism for proton transport, the hopping mechanism for electron conduction, and other charge transfer (CT) pathways. Strategies that are employed to improve photoswitchable conduction are elaborated. In the end, this work discusses ongoing challenges and provide an outlook into potential future directions for efficient property implementation in new materials and devices.**

## 1. Introduction

Light is a powerful tool for driving the discovery and development of new advanced functional materials due to its specific interactions with matter at the atomic, molecular, and nanoscale levels. Among its advantages over other external stimuli are remote control, low energy consumption and precision. This has enabled the discovery of numerous interesting phenomena and materials whose properties, such as conductivity, can be reversibly switched on and off by light absorption.[1–4] However, photoswitching efficiency and its speed, materials structural stability, photodegradation, crystallinity and tunability were still the matter of extensive optimizations. Therefore, new classes of materials for the remote control of electron and proton conduction properties and the photoswitching of responses were investigated more intensively over the past few years. Photoswitching of proton conductivity is particularly interesting because it opens the door to advanced applications in low-power, reconfigurable computing (particularly in complex logic gate architectures, where light-gated conductivity enables dynamic protonic logic operations and neuromorphic circuit behavior).[5] proton exchange membrane fuel cells[6] with on-demand proton conduction reducing standby energy losses, or bio-electronic devices with optically triggered, non-invasive, biomimetic proton pumps[7] for implantable systems, synthetic biology interfaces[8] or pH-regulated microreactors[9] with better stability and modularity than achieved using biological materials.[10] Efficient photoswitching of electron conductivity allows for light replacing electrical gating for wireless reconfiguration in optically gated transistors used in sensing, photodetectors, optical switches, optoelectronic circuits or photonic computing elements, as well as for reconfigurable memory and logic essential for adaptive computing, neuromorphic systems, or programmable logic arrays.[11–15] Thus, well-designed and efficient photoswitchable materials with remotely controlled photoswitchable conduction and high on/off ratios align with the demand for energy efficient, next-generation flexible and neuromorphic electronics, as well as smart materials for personal healthcare.

Light activated switching of electronic properties and reversibility of responses are permitted by photoswitchable molecules that undergo reversible structural rearrangements upon external light stimuli (**Figure 1**). Reversibility depends on the stability of the photogenerated state and is permitted if the new configuration is less stable, thus the return to the original state occurs upon a removal or a change of the stimulus.[16] With this respect, thermally reversible (T-type) or

H. Pacheco Hernandez, W. Wenzel, M. Kozlowska
Institute of Nanotechnology (INT)
Karlsruhe Institute of Technology (KIT)
Kaiserstraße 12, 76131 Karlsruhe, Germany
E-mail: mariana.kozlowska@kit.edu
S. Hecht
Department of Chemistry & Center for the Science of Materials Berlin
Humboldt University Berlin
12489 Berlin, Germany
L. Heinke
Physical Chemistry
Institute of Chemistry and Biochemistry
Freie Universität Berlin
14195 Berlin, Germany
The ORCID identification number(s) for the author(s) of this article can be found under https://doi.org/10.1002/adfm.202512262



**DOI: 10.1002/adfm.202512262**

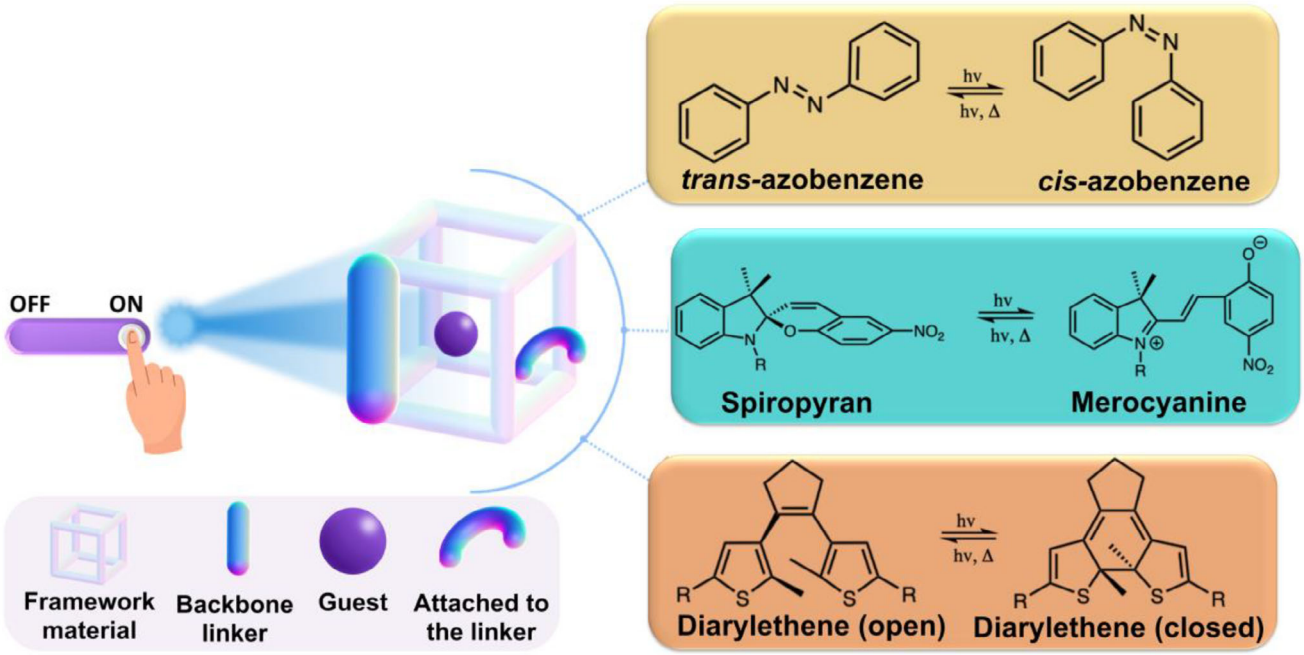


**Figure 1.** Photoswitchable molecules are commonly incorporated into framework materials in three different ways: i) as backbone linkers, ii) as guest molecules, and iii) attached to the linker. Diverse molecules were reported and summarized elsewhere.[28,30–35] Here, AB, SP and DAE are depicted as examples.

photochemically reversible (P-type) photoswitches are known.[17] One of the key benefits of photoswitches is that they rely on light as the primary stimulus, which is both precise and non-invasive, for the activation of structural changes.[18] A key prerequisite is understanding the specific wavelengths and conditions needed to induce these changes, permitting tailoring and modulation of their photoresponse.[19] The photoisomerization mechanisms of photoswitches can be categorized as (*E/Z*) isomerization or ring closing/opening transformations. (*E/Z*) isomerization involves the transition between *E* (entgegen) and *Z* (zusammen) configurations around a double bond. Thus, this type of isomerization does not include the making or breaking of any bonds but a distinct arrangement of atoms around the double bond, for example, the observed *cis* to *trans* changes in azobenzene (AB).[20] On the contrary, ring transformations involve bond breaking and formation within a molecular ring system. This mechanism has been observed for: spiropyrans (SP), diarylethenes (DAE),[21] DASA (Donor–Acceptor Stenhouse Adducts),[22] dihydroazulene (DHA)-vinylheptafulvene (VHF),[23] dimethyldihydropyrene,[24] fulgides and fulgimides.[25] Moreover, fulgimides can switch between different forms (*E*, *Z*, and closed-ring) depending on the light exposure. Overall, photoswitches offer a wide range of structural modifications and capabilities, making them attractive components to integrate into functional materials and devices.

Despite all the interesting functionalities, these molecules present certain limitations. For instance, in polar environments, many photoswitches do not dissolve well, or they often aggregate, which negatively impacts their absorption and emission properties and limit photoconversion.[19] This hinders the applicability of photoswitches in the solid state for electronic devices, sensors, memristors, etc. since their motion is restricted and the structural changes essential for the photoswitching are not permitted.[26,27] To overcome these limitations, photoswitchable molecules have been incorporated into nanoporous framework materials such as metal-organic frameworks (MOFs), covalent organic frameworks (COFs), Zeolitic Imidazolate Frameworks (ZIFs), and porous aromatic frameworks (PAFs) as guest molecules, backbone linkers, or attached to the main linkers (e.g., side groups), as schematically depicted in Figure 1. The crystalline nanostructure of these materials allows a precise control over intermolecular distances and pore size to prevent steric hindrance effects,[28,29] facilitating the use of photoswitches in the solid state with improved photoconversion, eliminating the need for solvents. The resulting solids can be grown as crystals or be epitaxially deposited on surfaces (e.g., thin films or surface-mounted MOFs, i.e., SURMOFs),[30] allowing for diverse harvesting of the photoswitchable responses.

In the past decade, investigations aiming toward the understanding the reversible photoisomerization of the photoswitchable linkers incorporated into different framework materials,[29,36–46] including isomerization efficiency and kinetics in systems like ZIF[40] and MOF[39,41,47] have been reported. More recent studies have explored the structural rearrangements of photoswitches for applications such as controlled cargo release[46,48–50] or controlled gas adsorption,[51] among others.[52] Beyond the structural diversity of photoswitches in different isomeric states, their electronic properties can also vary. For instance, one isomer may exhibit a higher tendency for charge transfer, facilitating charge carrier migration and enhancing the material's conductivity, while the other does not.[53] Moreover, different photoisomers can interact differently with or within the framework materials, leading to distinct material

 

responses.[54] Therefore, the photoswitching properties of framework materials with implemented photoswitches have been intensively investigated lately[28,30–32,55] and some recent reviews in this regard provide a summary of different pathways that have been explored.[56–58] However, the overview of conduction photoswitching in frameworks and the explanation of mechanisms of attained functionalities with the relation to the framework type have not yet been adequately addressed. In this review, we address studies focused on the photoswitchable responses of framework materials to reversibly control electron, proton and other ionic conductivity under light stimuli, and provide insights into the mechanisms involved in their functionality. We explain ongoing limitations, the envisioned role of molecular design for performance optimizations, and provide strategies aimed at advancing the conduction photoresponses of framework materials.

## 2. Framework Materials

Framework materials are a class of materials defined by their porous, lattice-like structures, which are typically crystalline. These materials are commonly classified based on their composition (e.g., hybrid, containing organic linkers and metal nodes, or purely organic frameworks) and bonding characteristics, with their coordination networks extending across different dimensionalities (e.g., 1D, 2D, 3D).[59] The primary categories of hybrid frameworks include MOFs,[32] with ZIFs[59] and MOF films like SURMOFs as important sub-groups.[60] COFs are well known in the class of pure organic framework materials,[61] other members of this classification include PAFs, Hydrogen-Bonded Organic Frameworks (HOFs),[62] Supramolecular Organic Frameworks (SOFs),[63,64] Porous Organic Frameworks (POFs)[65] and Halogen-bond Organic Frameworks (XOFs).[66] All materials mentioned have gained immense popularity with intense research efforts driven by their highly tunable properties and promising applications across various fields. For instance, size of pores, topology and microstructure of frameworks were demonstrated to be controllable by the linker length, interpenetrated structures, acidic or basic functional groups, reactivity of functional groups, second building units, etc.[67] This is extremely important for catalysis, where, for example, MOFs have been extensively studied due to their tunable active sites and pore environments. Similarly, COFs, due to their high surface area, tunable pore size, and chemical stability, have shown promising applications such as targeted and controlled drug release, as well as improving the sensitivity and selectivity of electrochemical biosensors.[68] However, electronic responses of framework materials are known to be limited in most cases, thus not all framework classes are equally investigated with this respect. For example, electronic properties of MOFs are restricted by their porous structure and inefficient electronic coupling, while ZIFs do not have highly conjugated structures necessary to create pathways for electron transport. This could be overcome by careful tuning of conduction pathways and adapting the topology of the framework. In this way, stacked 2D materials permit smaller intermolecular distances and increased conductivities in a specific direction.[57] Thus, 2D frameworks are recognized with an often larger conductivity than typical 3D frameworks because they enable shorter intermolecular distances and better electron density delocalization.[56] However, the controlled organization of donor-acceptor pairs within spatially continuous networks of frameworks containing guest molecules is also known to enhance the photoconduction on/off ratios resulting from efficient exciton separation and charge transport within donor and acceptor domains.[69]

Photoresponsive molecules in specific framework classes were used to advance the applicability of these materials for sensors, photodetectors, photoreactors, optical switches, memory and data storage devices,[28,31,70,71] and in emerging fields like optical computing.[72,73] However, a strong focus was given to light-activated conduction, where chromophores in frameworks permit the change in conduction properties and photocurrent, however without reversible structural changes in the organic linker itself.[31,69] Consequently, photoswitching between light-controlled "on" and "off" states was not possible, and the photoresponse was irreversible in its switching characteristics. For applications such as rewritable memory, optical switches, or adaptive sensing platforms, reversibility is essential to ensure repeatable and controllable photoresponses.[73,74] Thus, we focus below exclusively on framework materials that exhibit light-induced photoswitching responses, which are enabled by reversible structural changes in photoswitches. We discuss their conduction characteristics, the nature of their photoresponses, and performance upon assembly in frameworks. To highlight the factors influencing photoswitching and the diverse strategies reported for integrating photoswitches into frameworks, we first summarize some general concepts relevant to different classes of framework materials.

### 2.1. Photoswitchable MOFs

MOFs provide a well-defined crystalline structure that allows precise control over the arrangement of the photoactive molecules. Their porosity allows for the loading of chromophoric compounds into the pores or the integration as building blocks, which can lead to a more pronounced optical response compared to free molecules in solution.[31]

#### *2.1.1. Photoisomerization in MOFs*

Many studies have focused on the photoisomerization of ABs,[38,39] SPs,[36,44] DAEs[75,76] and, recently, DASA[45] in MOFs,[5,9,30,48,74,77] with azobenzene being the first photoswitchable linker incorporated into a porous MOF in 2011 by Modrow et al.[39] In 2013, Hermann et al. reported a MOF that included AB as a guest molecule and exhibited a higher switching efficiency compared to bulk solid-state azobenzene.[38] Although the photoisomerization of the azobenzene integrated as the side group of the linker molecules in the MOF structure can be sterically hindered upon specific assembly, Wang et al. experimentally and theoretically demonstrated the photoswitching of azobenzene side group in MOFs with layered structure and pillared connectivity.[29]

Photoisomerization kinetics in MOFs and photoswitching by the integration of other photoswitchable molecules such as SP, hydrazone, and DAE derivatives, and MOF confinement effects on photoisomerization speed, reversibility, stability, and

spectroscopic behavior were also investigated. For example, Thaggard et al.[78] showed that sterically demanding SP derivatives can boost the photoisomerization rate in rigid MOF matrices up to 1000 times compared to the same molecules in solution. However, chemical interactions, particularly host-guest effects and metal-photoswitch interactions, as well as steric effects and framework flexibility play a crucial role in determining the conversion efficiency of photoswitchable MOFs and the switching behavior.[73,79,80] For instance, SP functionalization in MOFs like MOF-808 demonstrated that host polarity and structural changes affect photoswitching efficiency and adsorption properties, with SP incorporation increasing $CO_2$ uptake but hindering reversibility due to stabilization within the pores.[81] Similarly, Schwartz et al. found that SP encapsulated in MOF-5, MIL-68(In), and MIL-68(Ga) exhibited reversible photoswitching, but the efficiency and kinetics depended on the polarity of the host framework.[79]

The way a photoswitchable molecule is incorporated into a MOF (e.g., as a guest, attached to the linker, or as a backbone linker, see Figure 1) also affects its switching efficiency, which is related to the differences in steric factors, pore confinement, and structural flexibility.[26] For backbone linkers, photoswitches with minimal structural changes upon isomerization are preferred, for example, DAE-based linkers, because the photoisomerization process (ring-opening/closing) occurs within the plane of the molecule imposing only minimal changes in the structure.[28] In contrast, for larger structural changes such as those in AB, the *cis*-to-*trans* photoisomerization is hindered due to the large geometrical rearrangements.[39] Significant structural changes are more feasible when photoswitches are attached to the linker[82] or introduced as guest molecules.[28] However, the latter approach, while simplifying synthesis, may lead to steric hindrance if the MOF pores are too small for effective photoisomerization.[80] Steric hindrance has been linked to asymmetrical photoisomerization effect, where the forward transition occurred significantly faster than the reverse.[51] For example, in some MOFs, switching in one direction can take as little as 10 min, while the reverse process can take over an hour.[52] A similar observation was reported for a metal-porphyrin framework integrating a DAE derivative, bis(5-pyridyl-2-methyl-3-thienyl)cyclopentene (BPMTC), as a backbone linker, where the closed-to-open transition was approximately 45 times slower than the reverse process.[83]

Some studies have demonstrated that thin-film MOFs can achieve significantly faster switching than the bulk ones.[84,85] It has been suggested that the high molar attenuation coefficient in photoswitches, which describes how strongly a species absorbs and thereby attenuates light, may limit the depth of light penetration in bulk framework materials (although in other classes of photoswitchable materials, penetration depths exceeding 1 mm have been realized).[86] This prevents efficient photoisomerization throughout the entire structure[31] in addition to isomer competition and photostationary state effects, known to decrease photoconversion.[86] In general, light penetration depth in material depends strongly on the wavelength of light and how strongly the material absorbs that wavelength. Strong absorption, particularly at shorter wavelengths, that are, indeed, often used for photoswitches,[87] results in a smaller penetration depth.[88] In line with this, Danowski et al. reviewed different photoresponsive porous materials and pointed out that photoisomerization in bulk is often confined to the surface due to scattering and limited light penetration, restricting switching throughout the framework.[35,89] In their paper, they provided some strategies to address this challenge. For example, growing MOFs as thin films, where thickness can be controlled, has been proposed instead of bulk materials, as it reduces steric hindrance and enhances light accessibility.[90] In line with that, Zhang et al. demonstrated improved photochromic properties, reversibility, and stability in a nitrobenzospiropyran-embedded MOF thin film.[44] Similarly, Fu et al. incorporated AB into HKUST-1 thin films, achieving high orientation and efficient guest encapsulation through a layer-by-layer growth method.[91] For an azobenzene MOF film, Jiang et al. estimated the light penetration depth, defined as the depth at which the light intensity in the material decreases to 1/e (~37%) of its original value, to be on the order of hundreds of nanometers.[30] Thus, thick MOF films (much thicker than 1 µm), or MOF materials in the form of pellets or large crystals, are illuminated and photoswitched only at the outer part of the material and large shares of the material remain in their dark state. As a result, not only the framework topology and strategies of photoswitch incorporation reflect the light-responsiveness of framework materials, but also the form of the processed material.

### 2.1.2. Photoswitchable MOF Films

Among MOF films, surface-mounted metal-organic frameworks (known as SURMOFs), synthesized directly on surfaces by layer-by-layer epitaxial growth,[92] provide an ordered, crystalline structure films, facilitating more controllable incorporation of photoswitches and tuning of their densities in a material.[30] Several studies have shown that integrating photoswitchable molecules as guests or linker side groups support efficient, reversible photoisomerization when sufficient free space is available to minimize steric hindrance. An important number of contributions have studied the photoisomerization process of AB in SURMOFs,[29,46] where reversible photoisomerization with approximately 64% conversion efficiency was reported in most cases. In addition, it was concluded that if steric hindrance is avoided, azobenzene switching occurs efficiently regardless of pore size or linker positioning.[93]

Reversible photoswitching, showing no sign of photobleaching or degradation after three irradiation cycles was also reported for fluorinated azobenzene attached to the linker ($F_2$AzoBDC) in $Cu_2(F_2AzoBDC)_2$(dabco) SURMOF with loaded butanediol[54] (see **Figure 2a** left). A decrease of the conductivity (i.e., seen by the Nyquist plot of the impedance depicted in Figure 2a bottom-right) in the *cis* state was observed upon irradiation with green light, that is, switching to the "off"-state by 530 nm inducing the *trans*-to-*cis* transition. The reversible photoswitching to the "on"-state occurs by 400 nm inducing the *cis*-to-*trans* transition. Thus, the reversible current and conductivity switching of guest molecules, such as 1,4-butanediol and 1,2,3-triazole, was explained to be dynamically controlled by the *trans* to *cis* isomerization of the SURMOF. We explain the conductivity switching in this MOF in detail in Section 3.

Kanj et al. studied $Cu_2$(e-BPDC)$_2$(dabco) SURMOF with SP-functionalized linker (e-BPDC denotes 2-ethynyl-[1,10-biphenyl]-4,40-dicarboxylic acid) to achieve photomodulation of proton

 

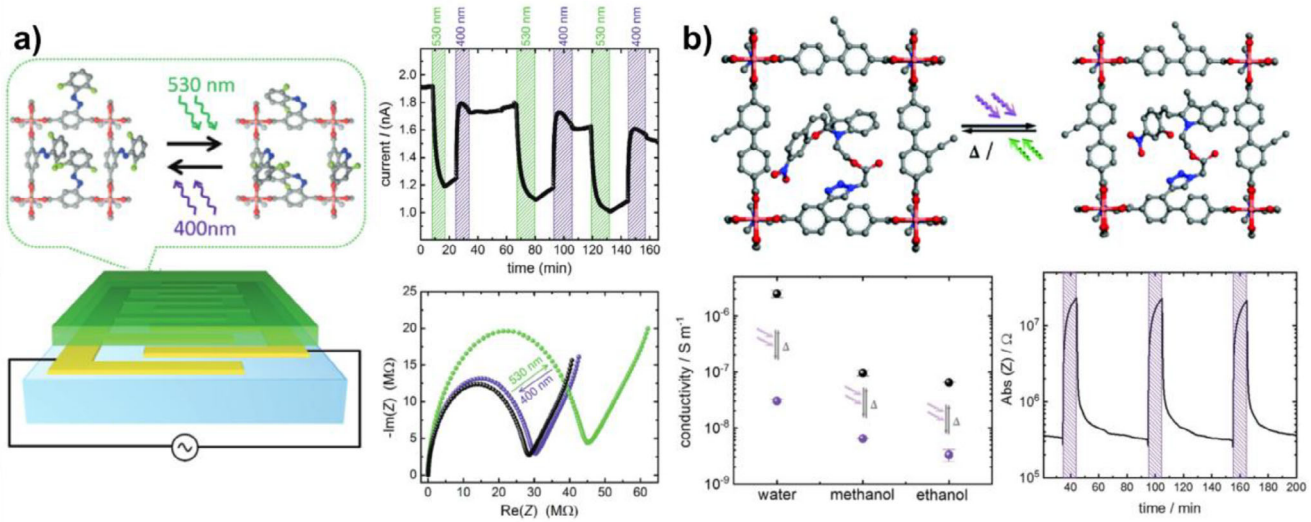


**Figure 2.** Proton conduction photoswitching in a) $Cu_2(F_2AzoBDC)_2(dabco)$ SURMOF with azobenzene integrated as a side group and b) $Cu_2(SP\text{-}BPDC)_2(dabco)$ with modified SP attached to MOF linker. For a): Three switching cycles of the MOF loaded with butanediol at 1 V and 1 Hz show the change in current upon irradiation with green light (530 nm), inducing *trans*-to-*cis* isomerization of the azobenzene groups (top right). Nyquist plot of the impedance (*Z*) of the MOF loaded with triazole: data in black represents the pristine sample (*trans*); data in green and violet indicate the *cis* and *trans* states after irradiation with green and violet light, respectively (bottom right). For b): MOF conductivity with different protic species loaded (water, ethanol and methanol) with results for the SP form shown in black and for the merocyanine (MC) form shown in violet (bottom left). Absolute value of impedance *Z* of the MOF with loaded water (bottom right). Figure a) adapted with permission from ref. [54] Copyright 2018. Published by John Wiley and Sons. Figure b) adapted with permission from ref. [94] Copyright 2020. Published by Royal Society of Chemistry.

conduction.[94] The UV light induced isomerization of SP to the MC form led to a substantial decrease in proton conductivity (i.e., by nearly two orders of magnitude, see Figure 2b) due to the strong binding of guest molecules to the MC isomer. Therefore, reversible differences in conduction could be achieved. Finally, they reported that photobleaching, which is usually caused by dimerization of SP, was prevented by anchoring SP to the MOF scaffold. The underlying mechanism behind the distinct photoresponse of this MOF film is explained below.

Recently, Klokic et al.[95] reported reversible photoswitching in Zn-based MOF films (Cl-DMOF-1) with AB incorporated into the pores. The use of chlorinated terephthalic acid and dabco as ligands yielded 3D-oriented MOF crystals with increased rigidity due to chloro-substitution. By controlling the growth time, they demonstrated that film behavior can be modulated, thereby influencing the photoresponse. Entirely rigid frameworks were obtained within short reaction times (10–60 min), resulting in the absence of AB isomerization in the films. Prolonged growth under intermediate times (90 min) produced more flexible heteroepitaxial films capable of reversible photoswitching. In contrast, extended growth (180–270 min) yielded films with lost epitaxial alignment and bulk-like (inhomogeneous) structuring, which hindered light penetration, thus impeding their photophysical characterization.

### 2.1.3. Photoswitching in ZIFs

ZIFs are a subclass of MOFs that have zeolite-like topology due to the similarity in the tetrahedral coordination of metal ions (e.g., $Zn^{2+}$ or $Co^{2+}$) with imidazolate linkers (Im), mimicking the Si–O–Si bond angles in zeolites. While ZIFs share some structural and thermal stability features with zeolites, they are still categorized as MOFs because they are built from metal nodes and organic linkers.[96] The number of references that include photoswitchable molecules in ZIFs is rather low. In comparison with MOFs, which offer a wide range of linker and metal combinations, ZIFs are primarily composed of zinc or cobalt ions and imidazolate-based linkers. This restricted chemical diversity can limit the design flexibility needed for incorporating photoswitchable units. Moreover, while MOFs can be tailored with a wide range of pore sizes and surface areas, ZIFs typically exhibit pore diameters which generally range from ≈5 to 16 Å with small crystallographic apertures between 2 and 5 Å due to their zeolite-like topologies.[97] As pointed out above, this can hinder the integration of photoswitches into their structure and the respective photoconversion performance.

The azobenzene-based molecule incorporated as backbone linker in the ZIF material isostructural to ZIF-8 was studied by Bernt et al.[40] The photoswitching was partially reversible, but the *cis* to *trans* isomerization cycle did not fully recover the original state after multiple cycles. They reported the photobleaching and steric hindrance effects to limit the full recovery, suggesting other approaches for positioning the photoswitchable molecule within the confined ZIF structure to be more efficient for improving the reversibility of the photoisomerization reaction. It was further investigated by Liang et al. in 2020 in a light-responsive ZIF-8 with high on/off photoswitchable proton conductivity,[7] where sulfonated spiropyran (SSP) was incorporated as guest. The resulting SSP@ZIF-8 hybrid membrane demonstrated reversible photoswitching with an on/off ratio of $2.8 \times 10^4$, and a fast response time of 5 s. We explain the properties of this material in Section 3.1 and 3.2.

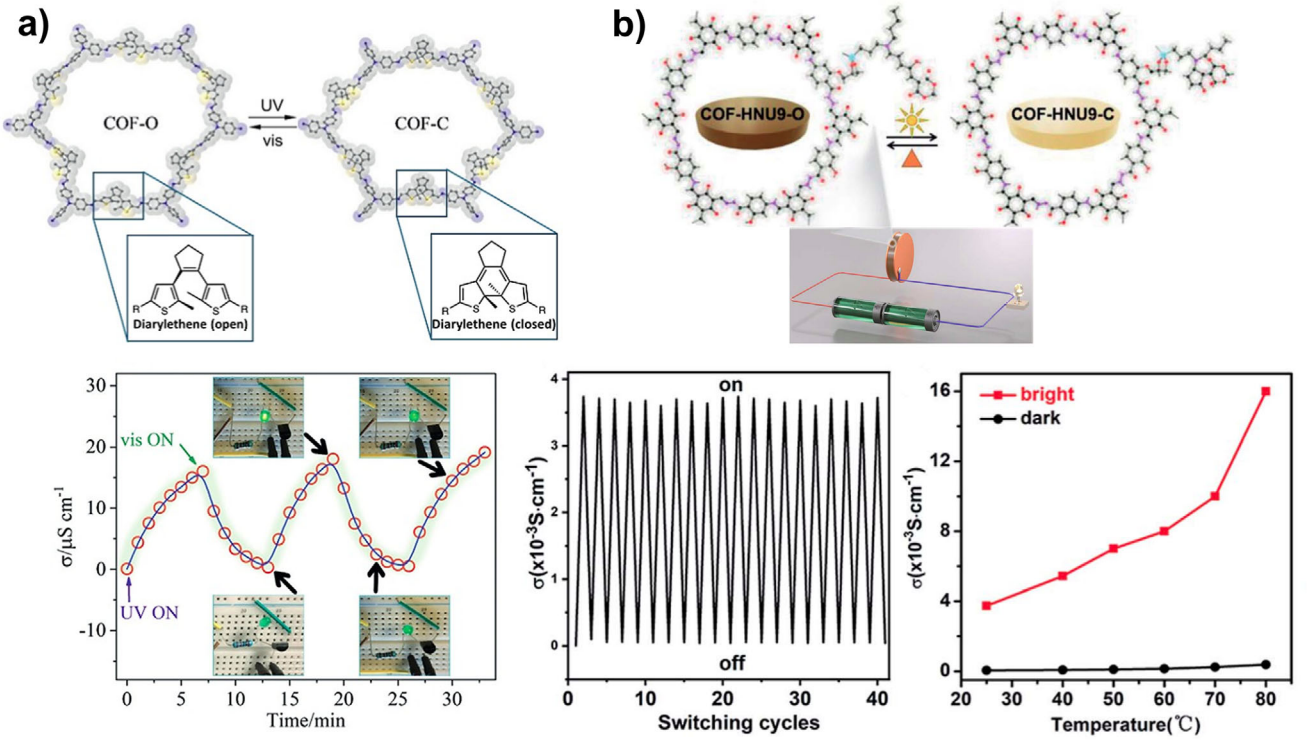


**Figure 3.** Schematic representation of selected strategies for integrating photoswitches into COF materials: a) DAE as backbone linker in COF-O (open ring) and COF-C (closed ring) for photoswitching of electron conduction (top panel) and cycles of conductivity changes upon repeated light switching (bottom panel).[105] b) DASA as side group in COF-HNU9[6] for photoswitching proton conduction (top panel). Photoswitching cycles of the COF-HNU9 film under light on/off at 25 °C and 98% RH and the temperature dependence of proton conductivity at 98% RH (bottom panel). Figure a) adapted with permission from ref. [105] Copyright 2019. Published by John Wiley and Sons. Figure b) adapted with permission from ref. [6] Copyright 2022. Published by Royal Society of Chemistry.

### 2.2. Photoswitchable COFs

COFs are crystalline, porous polymeric materials known for their structural integrity, high surface area, and design flexibility. Their 2D networks can be precisely tailored using a variety of organic building blocks. COFs comprising efficient $\pi$-conjugated structures facilitating efficient electron transport both within and between layers (e.g., based on phthalocyanine or porphyrin units) permit the obtainment of conductive materials, which are especially valuable for applications requiring high electrical conductivity.[98,99] In general, the conductivity of COFs can be enhanced by dopants embedding, however, unlike many MOFs, there are presently less studies on COF with photoswitching electronic responses. It is likely due to relatively good conductivities of $\pi$-conjugated COFs, ranging between $\approx 10^{-12}$ to $10^{-1}$ S m$^{-1}$ for intrinsically conductive frameworks,[100,101] and reaching values of $\approx$100 S m$^{-1}$ for doped COFs (e.g., $I_2$-doped).[102]

Shustova et al. have previously reviewed the dynamically controlled electronic properties of stimuli-responsive materials with different dimensionalities, including COFs materials.[32] They also managed to tune the electronic structure of a COF as function of an external stimulus by adding SP as a guest molecule in the pores.[103] They observed that upon UV irradiation there is a color change from pale yellow to dark red or brown indicating the transformation from closed SP to open MC. This led to a 39% increase in conductivity due to the $\pi$-electron delocalization present in MC, which can facilitate better charge transport within the COF. Yang et al.[104] reported that deposition of the organic semiconductor DPP4T on a 2D COF (BDFamide-Tp) enhanced its conductivity via interfacial doping, and subsequent encapsulation of SP enabled a photoswitchable electroactive response. It showed stable and reversible conduction photoswitching for at least 30 cycles without photodegradation and the output current in the on and off states of $1.2 \times 10^{-6}$ A ($V = 10$ V) and $1.2 \times 10^{-8}$ ($V = 10$ V), respectively. This resulted in a conductivity ratio of 2 orders of magnitude between the on and off states of the device. We discuss the mechanism of such a response in the next section.

In most reported cases of photoswitched COFs materials with photoresponsive molecules integrated either into the COF backbone or as pendant groups, linkers that undergo relatively small structural changes upon light irradiation, such as DAE-based building blocks, have been applied.[35] For example, 1,2-bis(5-formyl-2-methylthien-3-yl)cyclopentene was used as a covalently integrated building block in COF (see **Figure 3a**) obtained by Yu et al.[105] It demonstrated reversible photoisomerization between the open and closed-ring forms upon exposure to UV and visible light, respectively. The material exhibited excellent cyclability and a remarkable 200-fold increase in electron conductivity un-

der UV irradiation, attributed to the extended $\pi$-conjugation in the closed-ring isomer.

In 2022, Chen et al.[6] reported the reversible proton conduction of the photoresponsive COF named COF-HNU9, where DASA was incorporated as pendant group (see Figure 3b) within the channels of a $\beta$-ketoenamine-based COF (as a side group). The closed form of DASA significantly improved the proton conductivity by promoting hydrogen-bond networks with water molecules inside the nanochannels. The authors reported no significant degradation after 20 switching cycles, confirming the reversibility of the process (see Figure 3b bottom left). However, they observed that the flexible DASA units might block the pore opening at low temperatures. In the "on" state, an increase in the proton conductivity was observed with rising temperature, under 98% RH (see Figure 3b bottom right).

The role of spatial freedom in COFs, allowing the effective structural change of photoswitches, and the importance of designing linker structures for efficient photoswitched response was pointed out by the study of Das et al.[106] They demonstrated the storage and release of rhodamine B dye by the hydrophobic azobenzene-based COF, called TTA-AzoDFP, in response to UV light exposure. Mechanical motions of azobenzene, incorporated as the pendant groups pointing toward the pore channels permitted reversible photoswitching process, maintaining performance over multiple cycles.

### 2.3. Photoswitchable HOFs

HOFs are porous 2D and 3D materials built from organic molecules that are held together mainly by hydrogen bonds. The characteristic feature of HOFs differentiating them from MOFs and COFs is the supramolecular nature of their self-assembly based on a weaker bonding than coordination or covalent bonds, permitting easier synthesis and higher reversibility, but less stable structures, especially under harsh conditions. In addition to hydrogen bonds, the assembly of HOFs is strongly influenced by other forces such as $\pi$-$\pi$ stacking and C—H$^{\cdots}\pi$ interactions,[107] thus HOFs can be further tuned to achieve enhanced stability. Liang et al.[108] prepared a hydrogen-bonded crosslinked organic framework ($H_C$OF) which was first assembled as a HOF and then stabilized via covalent thiol-ene crosslinking (like known in COFs) forming $H_C$OF-101. Single-crystal X-ray diffraction revealed large 1D pores (≈1.4 nm) and flexible crosslinkages, giving the material high stability and permanent porosity. A hydrazone photoswitch was post-synthetically loaded into the pores, where it exhibited reversible *Z*/*E* photoisomerization for at least five cycles, which could not be realized in the neat hydrazone crystal. The use of HOF in this case enabled multicycle fluorescence switching, thus, the authors highlighted $H_C$OF-101 as a promising material for solid-state optical information storage devices.

Gao et al.[109] reported two kinds of HOFs with post-synthetically modified unbonded carboxylic groups, which are often associated with unstable properties of HOFs, namely Tb-HOFs and HOFs-olefin, modified with $Tb^{3+}$ and 5-hexene-1-ol, respectively. With a loaded SP into these HOFs, they aimed to create a multi-stimulus-responsive fluorescent HOF with potential applications in advance time-resolved information encryption. Upon incorporating the fluorescent center $Tb^{3+}$, they demonstrated that this hybrid material (Tb-HOFs@SP) exhibited dynamic emission changes as a result of the fluorescence resonance energy transfer process between the donor (Tb-HOFs) and the acceptor (the MC form). Specifically, the emission color shifted from green to yellow and ultimately to orange with regulation of the UV irradiation time and could subsequently be reverted to its original state under white-light exposure. Thus, the dynamic fluorescence emission of Tb-HOFs@SP could be achieved. In addition, they demonstrated that the photochromic properties of spiropyran, including fading speed and fatigue resistance, were enhanced in the modified HOFs, specifically in HOF-olefin@SP. This enhancement originates from changes in pore polarity resulting from the modification of residual carboxyl groups. Since the polarity of the environment affects SP photoconversion, leading to faster SP-to-MC photoisomerization and stabilization of the MC state under more polar conditions, thereby hindering photoswitching cyclability, the reduction in polarity within the modified HOFs resulted in distinct differences in switching behavior. Specifically, the saturation times were 3 min for unmodified HOF@SP compared with 5 min for HOF-olefin@SP, while the fading times for the MC-to-SP transition were 50 min for HOF@SP and 30 min for HOF-olefin@SP. Moreover, fatigue-resistance studies revealed that HOF-olefin@SP showed the best performance even after five cycles.

Recently, Liu et al.[110] developed a photoresponsive HOF capable of solution-mediated reversible 2D-3D framework transformation by remote light irradiation. The synthesized 3D HOF (HOF-OF), comprising DAE and tetrakis(4-amidiniumphenyl)methane as building blocks connected by charge-assisted hydrogen bonds, showed photocontrolled reversible structural conversion to a new 2D HOF via solution processability. The authors explained that upon UV irradiation, DAE converted from the ring-open to ring-closed form, generating internal strain that was released through hydrogen bond breaking, resulting in reassembly, changing the initial 3D structure to a 2D HOF (HOF-CF). They reported that the open DAE form and regenerated 3D framework could be achieved reversibly with visible light. Upon loading the lanthanide complex into a HOF with emission overlapping the DAE absorption, they demonstrated reversible luminescence on/off switching of the material via a photochromic fluorescence resonance energy transfer process. The authors proved the functionality of this HOF as an invisible security ink and promising application for intelligent high-security anti-counterfeiting, where the irradiation with UV and visible light enables a higher level of anti-counterfeiting.

Despite the multiple advantages of HOFs and the diverse functionalities that can be programmed into these materials, the number of photoswitchable HOFs remains limited, and such frameworks have not yet been reported to exhibit light-switchable conduction properties. This highlights the importance of further exploring these materials with diverse types of framework functionalizations and photoswitchable molecules.

### 2.4. Other Photoswitchable Framework Materials

Beyond the most often investigated framework materials comprising MOFs and COFs, other framework types are known

to be adaptable for photoswitching. Their conductivity photoswitching remains largely unexplored, partly due to challenges related to the material's stability in comparison with MOFs and COFs. For example, Kundu et al.[111] reported photoresponsive PAFs and photoresponsive porous aromatic networks (PANs) with covalently linked SP inside the framework, allowing reversible photoisomerization in the solid state. After testing over 100 cycles, no significant photodegradation was observed under inert conditions, but degradation occurred in ambient conditions. The conversion efficiency depended on the SP loading, and the nanoporous environment facilitated efficient isomerization. In addition, Castiglioni et al. studied the modulation of porosity and gas uptake through bulk photoisomerization in porous switchable frameworks (PSF) with a bistable chiroptical overcrowded alkene as the photoswitchable molecule. The overcrowded alkene[112,113] was integrated into the framework backbone via its fluorenyl moiety (acting as the stator), while the naphthyl moiety (acting as the rotor) remained pendant in the pores, providing enough space for rotation. The material exhibited efficient and reversible photoisomerization in the solid state with no significant photodegradation. Yuan et al.[65] synthesized an azobenzene-functionalized POF that, through reversible *trans - cis* photoisomerization, enabled light-controlled change of pore size and $CO_2$ adsorption, which was reflected in a 10% decrease of the $CO_2$ uptake after UV irradiation. Almost full recovery was observed upon thermal regeneration with almost no decay after three alternating external-stimuli cycles, demonstrating the reversibility of the transformation as well as the reproducibility of the $CO_2$ storage-release process in this case. Sheng et al.[114] reported the synthesis of PSF by modular post-synthetic grafting strategy, enabling the successful and flexible introduction of SP pendant groups inside the porous network. They reported that the photoisomerization was reversible and efficient in the bulk solid state, which is a common challenge in other framework materials.

Recently, Jin et al.[115] reported crystalline 3D photochromic MOFs formed by assembling Metal-Organic Polyhedrons (MOPs), which represent assemblies of organic linkers and metal nodes, serving as supramolecular building blocks to build extended 3D MOFs. A photoswitchable DAE-based linker (1,5-Bis(2-methyl-5-(4-pyridyl)-3-thienyl)cyclopentane), coordinated with $Cu^{2+}$ or $Rh^{2+}$ metal nodes, was incorporated into two MOP-based MOFs, DUT-210(Cu) and DUT-210(Rh). More stable photoswitching cycling was reported for DUT-210(Rh) than for DUT-210(Cu), which degraded under high UV exposure. Steric hindrance and framework rigidity were shown to influence isomerization kinetics with Rh-based MOF having higher rigidity and faster switching. However, these materials are more likely to find relevant applications in kinetic design for optically driven motors, actuators, or biomedical release systems, rather than in conduction photoswitching.

In summary, in this section different strategies for photoswitchable framework materials were described, each with their advantages and limitations. Efficient photoconversion regulated particularly by the balance between sufficient conformational freedom, minimizing steric hindrance within the framework and material's fabrication form, for example, thin films or powders, were pointed out. Achieving high reaction reversibility, preventing photodegradation of photoswitches, and ensuring light penetration throughout the entire material permitted by thin film technologies were demonstrated as a promising pathway for the development of new light induced stimuli responsive materials. In the next section, we explain the conduction photoswitching functionality of reported framework materials and explain the mechanisms of underlying electronic responses.

## 3. Conduction in Photoswitchable Framework Materials: Types and Mechanisms

Although conductivity in framework materials has been studied extensively over the years, and photoisomerization behavior in such materials has been explored for the past decade,[39] the integration of photoswitchable molecules to enable on-command conductivity changes represents a more recent topic.[116] To the best of our knowledge, the first report of the light-induced conductivity switching in framework materials was published by Müller et al.[54] in 2018, addressing the proton conduction change in a SURMOF modified with azobenzene as a side group within the material. Shortly afterward, Garg et al. (same group) demonstrated on/off light-induced electron conductivity switching in the UiO-67 MOF with embedded SP as a guest through reversible SP-to-MC isomerization and stronger electronic coupling between MC species compared to SP species.[53] Since then, the topic has gained significant attention, and the number of studies has been continuously increasing (see **Figure 4**), reporting various conduction mechanisms and diverse strategies for improvement of an on/off conduction switching.

Since mainly two conduction types in framework materials have been investigated up to date, that is, proton and electron conduction, in the following section, we discuss them separately, explaining underlying mechanisms and microscopic parameters relevant for conduction photoswitching phenomena. Generally, protons are not free charge carriers; instead, they require hydrogen-bonded networks and proton donor/acceptor groups to move through the framework. This can occur via either the Grotthuss or the vehicle mechanism.[121] In contrast, electronic charge transport occurs either via hopping mechanism, where charge carriers (electrons or holes) move between localized states, or band-like mechanism, where charge carriers propagate through delocalized electronic states.[56] Moreover, charge transport mechanism at the borderline between the localized hopping and delocalized charge transport, that is, dynamically disordered, partially coherent transport regime, where carriers are transiently localized by molecular fluctuations but retain some delocalized character, is known.[122,123] Such mechanism was suggested for MOF frameworks due to frustrated rotation of linkers causing fluctuations of the electronic coupling and dynamic disorder.[124]

### 3.1. Proton Conduction

Proton conduction refers to the movement of positively charged hydrogen ions (e.g., $H^+$, $H_3O^+$, or even $NH_4^+$) in solution or through a material. For the framework materials, two main mechanisms are typically reported to describe this type of conduction: (i) the Grotthuss mechanism, which occurs when a proton hops between molecules, and (ii) the vehicle mechanism,

 

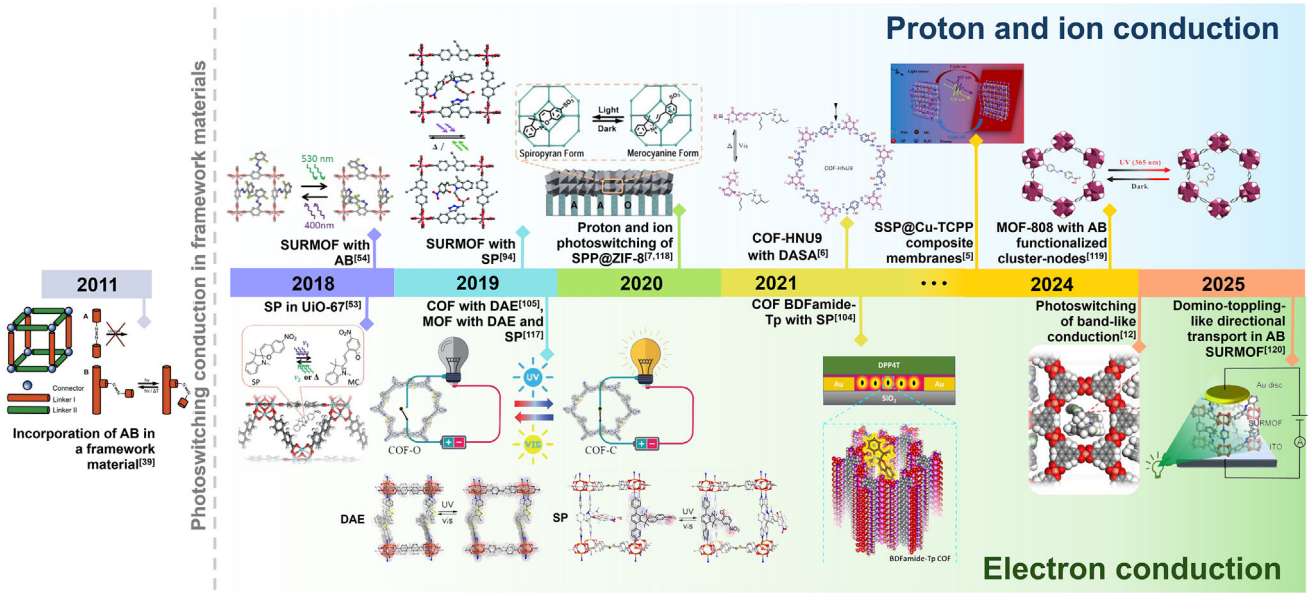


**Figure 4.** Timeline illustrating the development of light-induced conductivity switching in framework materials by the incorporation of different photoswitchable molecules. The materials summarized in the timeline are described in the text. Figures adapted with permission from ref. [39] (Copyright 2011, Royal Society of Chemistry), ref. [54] (Copyright 2018, John Wiley and sons), ref. [53] (Copyright 2019, John Wiley and sons), ref. [94] (Copyright 2020, Royal Society of Chemistry), ref. [105] (Copyright 2020, John Wiley and sons), ref. [117] (Copyright 2020, American Chemical Society), ref. [7] (Copyright 2020, John Wiley and sons), ref. [118] (Copyright 2020, Royal Society of Chemistry), ref. [104] (Copyright 2022, American Chemical Society), ref. [6] (Copyright 2022, Royal Society of Chemistry), ref. [5] (Copyright 2023, Royal Society of Chemistry), ref. [119] (Copyright 2024, American Chemical Society), ref. [12] (Copyright 2025, John Wiley and sons), ref. [120] (Copyright 2025, John Wiley and sons).

known for proton migration via a carrier molecule to which the proton is bonded, permitting the proton to move together with the carrier.[125] The main requirement for the Grotthuss mechanism is a continuous hydrogen-bonded network that allows proton hopping.[126] This process often involves activation energy < 0.4 eV, while the vehicle mechanism is related with higher activation energy, typically > 0.4 eV.[127,128]

Various factors impact the mobility of charge carriers in both proton conduction mechanisms in solution, however, in photoswitchable framework materials, in hydrous conditions, where water molecules are involved, temperature, humidity and loading of guest molecules were found to have the most effect. Temperature (e.g., < 85 °C) accelerates conduction, while relative humidity (RH) (e.g., > 90% RH) promotes the formation of dynamic hydrogen-bonding networks within the framework, facilitating proton hopping through diverse channels. In MOFs in anhydrous conditions, where water is absent, the critical factors determining proton conduction are charge carrier concentration, structure, acidity and the presence of alternative nonvolatile conduction medium (e.g., triazole, imidazole).[121,129]

The remote control of proton conduction by light was reported for the SURMOF film with a pillared-layered $Cu_2(F_2AzoBDC)_2(dabco)$ with o-fluoroazobenzene moieties attached to the linker (see Figure 2a) in 2018.[54] Two guest molecules, that is, 1,4-butanediol and 1,2,3-triazole, were loaded in this MOF and proton conduction was steered by *trans*-to-*cis* and *cis*-to-*trans* isomerization of azobenzene moieties and the differences in the hydrogen bridges formed between the guest molecules with the azo groups in the *cis* and *trans* states of the photoswitch. With the green light of 530 nm, 86% of the *cis* form was obtained, while with the violet light of 400 nm, conversion back to the *trans* form in 87% was achieved. Since the stronger bonding between the guest molecules with the *cis* state occurred, the mobility of the guest molecules decreased, resulting in a decreased proton conductivity. At room temperature, SURMOF with the azobenzene linkers in the *trans* state showed better conduction, that is, for butanediol the conductivity of $9.0 \times 10^{-6}$ S m$^{-1}$ and $6.1 \times 10^{-6}$ S m$^{-1}$ was obtained in the case of the *trans* and *cis* state, respectively, while for triazole the measured values were $1.2 \times 10^{-4}$ S m$^{-1}$ and $7.9 \times 10^{-5}$ S m$^{-1}$. Thus, by switching the state of the photoswitch in the framework scaffold, proton conduction triggered by guest molecules was altered and could be repetitively changed using different light. This study represents the role of hydrogen bonding dynamics between the guest molecules that controls conduction.

The light control of proton conduction in framework materials with spiropyran was reported too.[94] Here, using a copper-based SURMOF, $Cu_2(SP\text{-}BPDC)_2(dabco)$, functionalized with SP moieties via post-synthetic modification (PSM) was prepared (see Figure 2b). The infrared spectroscopy measurements indicated 0.83 photoswitchable moiety anchored in each MOF pore, that is, almost 1 per pore. The material exhibited a proton conductivity of $2.5 \times 10^{-6}$ S m$^{-1}$ in the SP form at room temperature and 93% RH. It showed a significant decrease upon UV-induced switching to MC with an on/off ratio of 82. A high switching yield (≈80%) of MC was achieved under 365 nm UV-light irradiation. The possibility of changing the proton conduction in this material was demonstrated using different guest molecules (i.e., water, methanol, and ethanol). The highest on/off ratio of 82 was observed for water. The switching process was fully reversible,

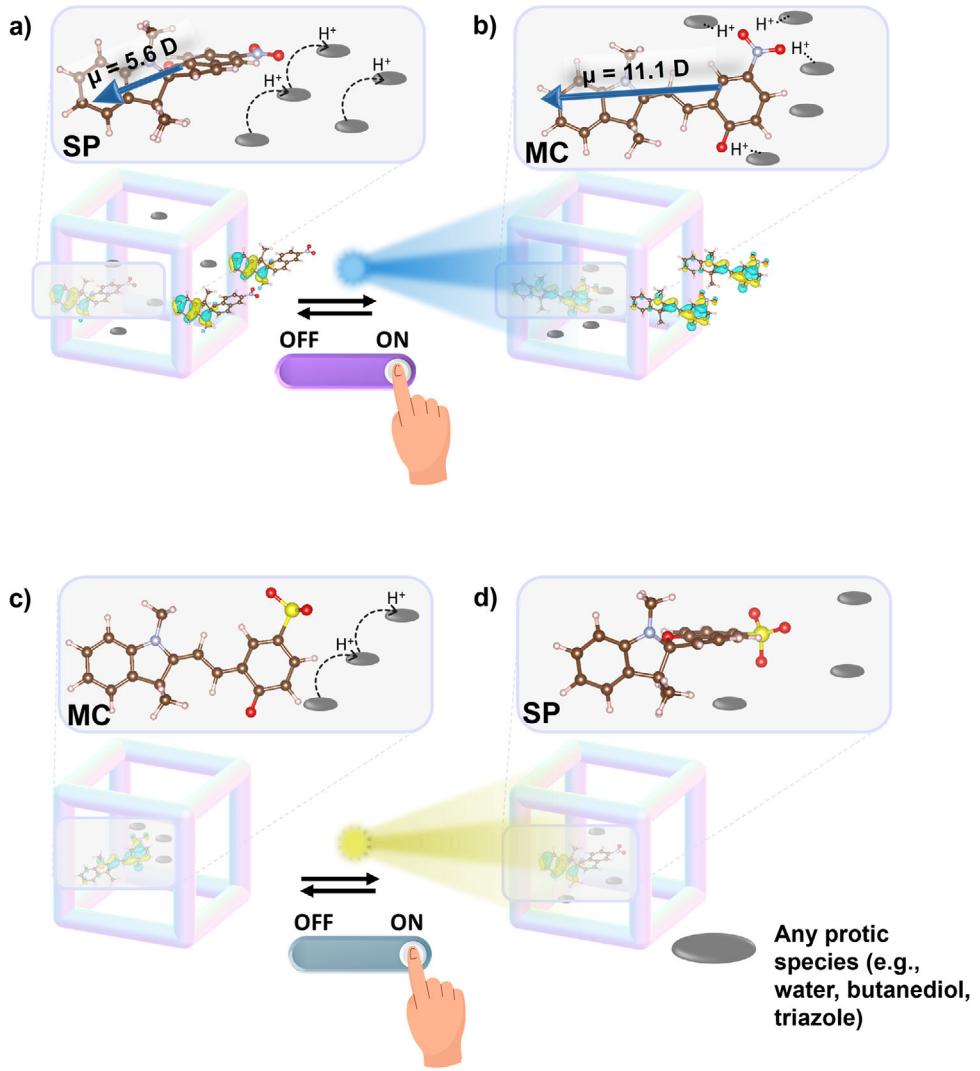


**Figure 5.** Light-induced modulation of proton conduction in SP-functionalized framework materials. The top panel schematically represents the nitro-substituted SP photoswitch (a) that was incorporated within the MOF scaffold upon PSM as reported in ref. [94] where the UV light was used for the SP-to-MC (b) conversion modulating proton conduction in $Cu_2$(SP-BPDC)$_2$(dabco) SURMOF (see Figure 2b). The role of hydrogen-bonded networks is highlighted. In the bottom panel, the photoswitching between thermodynamically stable MC form of SSP (c) loaded as guests in ZIF-8[7] and its conversion to SP (d) under visible light exposure is depicted. In both cases, additional protic species were embedded in the pores of the framework. Dipole moment was calculated using the gas-phase optimized molecules using CAM-B3LYP functional with the def2-TZVP basis set.

and no significant photobleaching was detected after multiple switching cycles. The study suggested that proton conduction between the guest molecules in the MC form of the MOF linker is impacted by strong hydrogen bonding between guest molecules and MC (schematically depicted in **Figure** 5b). Infrared spectroscopy results provided direct spectroscopic evidence that water guest molecules are strongly adsorbed, which is connected to a decrease in conductivity. Since the polarity of the molecule in the SP form differs from the one in the MC form, what is modulated by the change of the electronic structure and different dipole moments attained, for example, from 5.6 Debye for the nitro-substituted SP to 11.1 Debye for its MC form (marked in Figure 5), much stronger short-range binding of the guests to the framework with MC was present. The authors pointed out that the strength of such interactions is one for the reasons of the 13-times-higher switching effect in proton conductivity of ethanol in SP-MOFs (by a factor of 20) than in butanediol in AB-MOFs, switched only by a factor of 1.5.

In 2020, Liang et al. investigated the proton conductivity of a light-responsive ZIF-8 with sulfonated spiropyran (SSP@ZIF-8)[7] as a guest molecule. SSP is characterized by the MC form stabilized in the dark in polar environments, making MC the favored state, necessitating visible light for triggering ring closure back to the SP form (Figure 5c,d). It is known as negative photochromism.[130,131] The SSP in ZIF-8 was incorporated at different weight ratios (1%, 5%, 10%, and 20%) using a solid confinement conversion process at room temperature, starting from a composite thin film of zinc hydroxide nanostrands (ZHNs) and SSP. The authors reported that due to electrostatic interactions, the negatively charged SSP adhered to

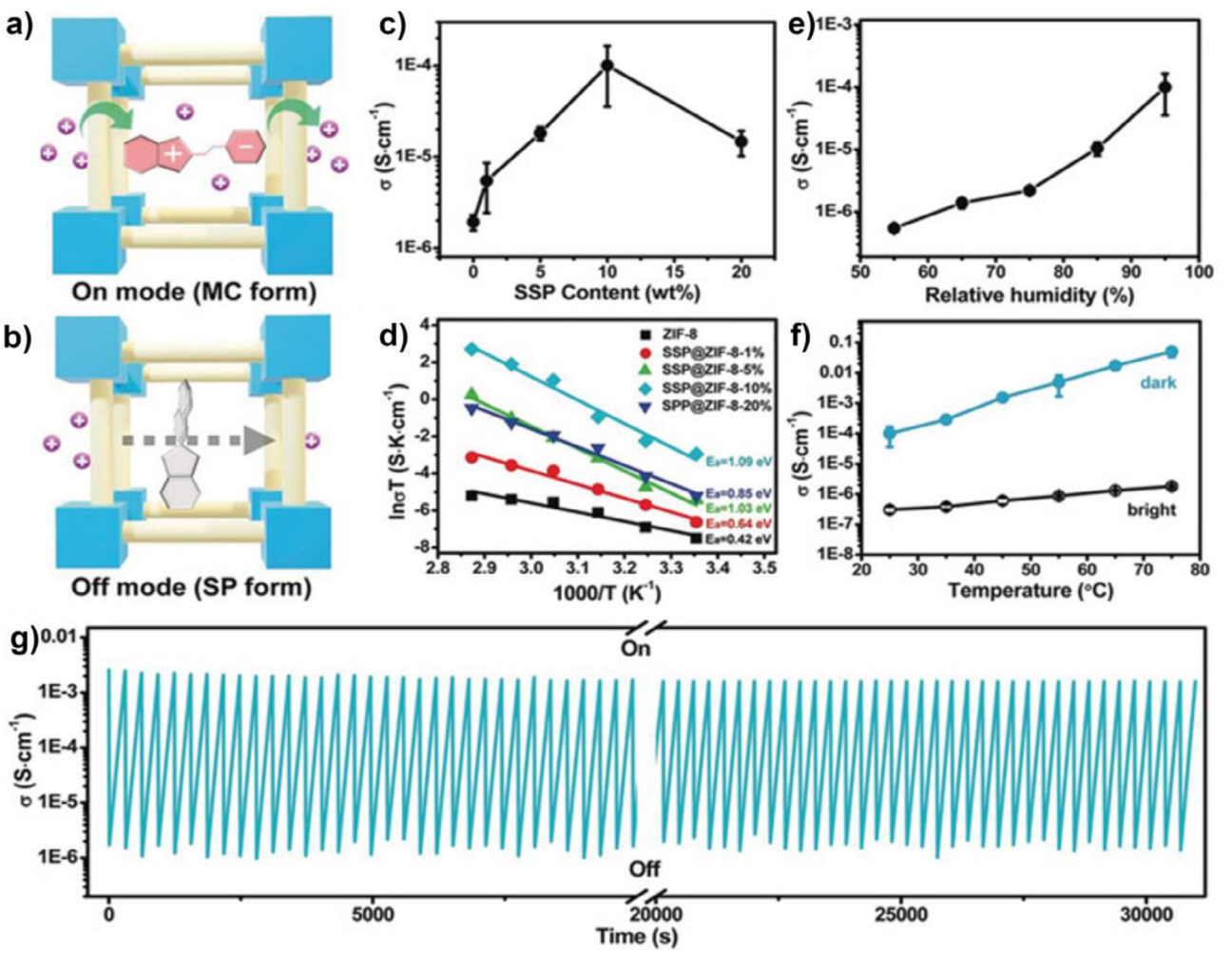


**Figure 6.** Photoswitching of proton transport in SSP@ZIF. a) and b) The schematic illustration of the possible transport mechanism in the presence of MC and SP forms of SSP. c) Measured proton conductivity of SSP@ZIF with different SP loading at 25 °C and 95% RH in the dark. d) Comparison of Arrhenius plots with different SSP content under 95% RH. e) Proton conductivity of SSP@ZIF-8-10% under different humidity and at 25 °C in the dark. f) Comparison of the proton conductivity of SSP@ZIF-8-10% under visible light (black line, SP form) and in the dark (blue line, MC form) with 95% RH. g) Reversibility cycles of proton conductivity of SSP@ZIF-8-10% membrane by turning on/off light illumination, measured at 55 °C and 95% RH. Figure adapted from ref. [7] Copyright 2020. Published by John Wiley and Sons.

the positively charged ZHNs, and during the transformation of ZHNs into ZIF-8, SSP became confined within the MOF cavities (see **Figure** 6a,b). Among the tested compositions, 10% SSP@ZIF-8 exhibited the highest proton conductivity and the photoswitching response at 75 °C and 95% RH with the conductivity under visible light (SP-form) of $1.8 \times 10^{-4}$ S $m^{-1}$ versus 5.0 S $m^{-1}$ obtained for the MC form (Figure 6c–f). The response time was measured to be 5 s and an on/off ratio of $2.8 \times 10^4$ was reported. Moreover, this material demonstrated reversible switching with no significant photodegradation even after 100 cycles. Liang et al. reported that SSP@ZIF-8 follows a mixed proton conduction mechanism, where activation energies range from 0.64 eV to 1.09 eV, depending on SSP loading. These values typically indicate a vehicle mechanism (> 0.4 eV), however, the authors proposed that Grotthuss (hopping) conduction also contributed, facilitated by hydrogen-bond networks formed by the MC form of SSP functional groups (phenol and sulfonate) and water molecules inside the MOF cavities (see Figure 5c). In general, the encapsulation of SSP reduced the effective pore space, making water diffusion more restricted, which was reflected in increased activation energy results with loading (Figure 6d). Despite this, SSP@ZIF-8 still presented high proton conductivity results thanks to the strong hydrogen-bonding interactions (between the MC form of SSP and water molecules). Interestingly, although the pristine ZIF-8 exhibited a low activation energy of 0.43 eV, explained by the authors as Grotthuss mechanism, its conductivity was two orders of magnitude lower than the SP-loaded (SSP@ZIF-8-10%). This suggests that even if proton hopping was in principle possible, the additional hydrogen-bonded networks between photoswitches and water in ZIF-8 permitted efficient conduction of SSP@ZIF-8.

Proton conduction in a copper-based MOF, Cu-TCPP (copper tetrakis(4-carboxyphenyl)porphyrin), modified with polystyrene sulfonate (PSS) and SSP to form PSS-SSP@Cu-TCPP composite

membranes was reported by Xue et al. in 2023.[5] The composite was synthesized via an in situ solid confinement method, using copper hydrogen nanostrands as the metal source. The measured proton conductivity in the dark, where MC-form was present, reached $1.37 \times 10^{-2}$ S m$^{-1}$ at 55 °C and 95% RH, showing on-off ratio beyond $10^3$ between the change to the SP form by applying 520 nm light. The authors explained that the reason for this observation was that the hydrophilic MC form (i.e., with significantly larger dipole moment, so higher polarity, as depicted for the nitro-substituted MC in Figure 5b) provided phenol groups that participate in the construction of a hydrogen bonding network, enhancing proton conduction and leading to an overall increase in the conductivity of the PSS-SSP@Cu-TCPP composite membrane, as explained for SSP@ZIF-8 above. However, upon irradiation at 520 nm, the SSP underwent photoinduced structural changes, transforming from the MC form to the less polar SP form, which, in addition, blocked the phenol groups from participating in hydrogen bonding, thereby decreasing proton conductivity. The study indicated that both Grotthuss and vehicle mechanisms contribute to proton conduction. The activation energy of 0.62 eV in the dark suggested that the vehicle mechanism dominated, as water molecules facilitate proton transport. However, as temperature increased, some water molecules escaped, causing a reduction in activation energy, suggesting a transition to a more Grotthuss-like mechanism, where proton hopping along a hydrogen-bonded network becomes more dominant.

More recently, a new study demonstrated the use of a different approach of anchoring photoswitchable units in frameworks. Liu et al.[119] grafted azobenzene-4,4′-dicarboxylic acid (AZOA) onto the $Zr_6(\mu3\text{-}O)_4(\mu3\text{-}OH)_4$ nodes of MOF-808 through the partial substitution of the terminal formate groups, creating a functionalized MOF-808-AZOA. They have shown that in the *trans* form of AZOA, there was no interaction between the terminal carboxyl groups of the photoswitch and the oxygen atoms of the Zr-based secondary building unit, permitting H-bonded networks between guest water molecules and AZOA increasing proton conductivity. Under UV light (365 nm), when the *cis*-AZOA was formed, it exhibited a much closer contact with the metal node, indicating the charge-assisted H-bonding interactions with the node instead of with the water molecules. In addition, the hydrogen atom in the terminal COOH group of AZOA should be more difficult to dissociate in this case, thus proton conduction in the *cis* state was decreased. Although conductivity values were not explicitly reported, the observed change in resistance indicated a reversible, light-controlled switching in proton conductivity. The *trans*-to-*cis* isomerization of AZOA resulted in the impedance increase from ≈15 kΩ (dark, *trans*) to ≈3 MΩ (UV, *cis*), representing a 200-fold change after 100 s.

A stimuli-responsive proton conductive COF (COF-HNU9) (Figure 3c) incorporating DASA within $\beta$-ketoenamine-based COF channels was reported by Chen et al.[6] the parent COF was synthesized via condensation of 1,3,5-triformylphloroglucinol and 4-aminosalicylhydrazide using a solvothermal approach, and DASA was anchored into the COF channels as a PSM. The DASA moieties underwent reversible open (COF-HNU9-O) to closed (COF-HNU9-C) photoisomerization upon visible light irradiation, and the structure reverted thermally upon heating. At 98% RH and 25 °C, the proton conductivity of COF-HNU9 increased by three orders of magnitude compared to the pristine COF upon visible light irradiation. At 98% RH and 80 °C, the conductivity reached 2.0 S m$^{-1}$. The switching process was reversible, and after 20 switching cycles no significant photodegradation or conductivity loss was observed. From the switching kinetics measurements, the photoisomerization from COF-HNU9-O to COF-HNU9-C was estimated to occur in approximately 120 min under visible light, while the thermal reversion back to COF-HNU9-O required 180 min at elevated temperatures. The activation energy of the pristine COF was 0.44 eV, indicating a mixed conduction mechanism in which both the Grotthuss and vehicle mechanisms could contribute. In the light-exposed COF-HNU9-C state, the activation energy decreased to 0.25 eV, consistent with a dominant Grotthuss-type conduction mechanism facilitated by strong hydrogen-bond networks. The hydrophilic properties of COF-HNU9-C were suggested to enhance proton transfer pathways, leading to higher proton conductivity upon light irradiation.

### 3.2. Ion Conduction

Beyond conduction photoswitching based on proton transport, ion conduction modulation (i.e., non-proton) controlled by light has been reported. For that, Liang et al. synthesized MOF-membranes ZIF-8 with incorporated SSP as a guest molecule (SSP@ZIF-8) at different weight ratios (1%, 5%, 10% and 20%).[118] The SSP@ZIF-8 membranes were constructed via a solid confinement conversion process from a composite thin film of ZHNs and SSP at room temperature. This material showed selective adsorption of $Li^+$ over other tested ions ($Na^+$, $K^+$ and $Mg^{2+}$) and demonstrated reversibility in ion conductivity upon light irradiation, with no apparent photodegradation (see **Figure 7a**). The best result was observed for SSP@ZIF-8-10% membranes with a $Li^+$ conductivity of $1.6 \times 10^{-2}$ S m$^{-1}$ (in the MC-form) and $7.1 \times 10^{-4}$ S m$^{-1}$ (in the SP-form) at 25 °C. Thus, the on/off ratio of 23 upon visible light irradiation was reported. The conduction mechanism was explained to be dominated by a hopping process, in which $Li^+$ ions hop between available binding sites within the channels. The activation energy for $Li^+$ transport was found to be lower in the MC state (0.51 eV) than in the SP state (0.56 eV), as shown in Figure 7b. This suggests that in the MC form (dark state), the oxygen atoms in the sulfonate and phenol groups of SSP serve as $Li^+$ binding sites, facilitating the hopping of $Li^+$ ions from site to site. In contrast, upon visible light irradiation, the phenol group is absent in the SP form, reducing the number of available binding sites and increasing the energy barrier for ion transport, thereby decreasing conductivity.

In this study, the authors reported significant differences in the on/off conductivity ratios of other cations (Figure 7c). In comparison to $Li^+$ with the highest photoswitched differences in conductivity, $Na^+$, $K^+$, and $Mg^{2+}$ were found to have lower values of 3.8, 1.7 and 1.3 in the SSP@ZIF-8-10% membranes, respectively. It indicates that the MC-SP isomerization impacts the conductivity of $Li^+$ more significantly, probably due to the different size of the $Li^+$ cation and larger differences in $Li^+$ binding energies to MC and SP forms. Thus, this study demonstrated not only photoswitching-modulated changes in conduction but also high ion selectivity, offering an interesting approach for design-

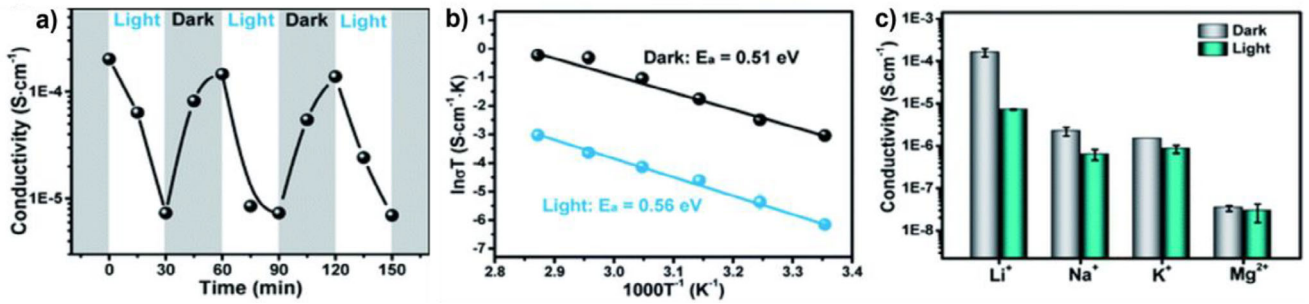


**Figure 7.** Light controlled ion conduction in ZIF-8. a) Lithium-ion conductivity in SSP@ZIF-8-10% upon different light exposure. b) Arrhenius plots of SSP@ZIF-8-10% for $Li^+$ transport in the presence of MC form (in dark) and SP form (with light) of SSP. c) The comparison of on/off switching ion conductivity of SSP@ZIF-8-10% membranes for different metal ions before and after visible light irradiation. Figure adapted from ref. [118] Copyright 2020. Published by Royal Society of Chemistry.

ing functional materials for the efficient extraction of lithium ions and the remote control of lithium-ion conduction, which could significantly advance the development of lithium-ion battery technologies.

### 3.3. Electron Conduction

Different pathways for electron transport in framework materials have been identified. In their extensive review on electrically conductive MOFs, Xie et al. grouped them according to the design strategy to: guest promoted, hopping, through-space, through-bond and extended conjugation.[56] In a simplified classification, these pathways can be divided into two main categories: (i) through-bond and (ii) through-space.[57] In the through-bond pathway, the electron transport involves coordination bonding between the MOF components, allowing charge carriers to move through continuous chains of bonds within the framework. The through-space pathways are triggered when the spatial separation between charge carriers exists and electronic properties are controlled by effects such as orbital overlap, $\pi$-$\pi$ stacking, noncovalent interactions or environmental effects modulating changes in the electronic levels. Thus, often the electron conduction pathways can be explained using principles from solid-state physics, where the mechanisms for electron transport depend on how electronic structure (band structure), degree of order, and interaction with the lattice or defects control charge motion. Here, two main charge transport mechanisms are known for framework materials, that is, band-like conduction and hopping conduction.

In band transport, electrons are free to move in continuous energy bands with delocalized charge carriers, allowing for barrierless movement across the material (see **Figure 8**a), leading to high electron conductivity. However, this transport mechanism is rare in framework materials and mainly occurs for specific topologies and chemical compositions of frameworks,[132–134] for example, with coupling between the metal nodes and organic linkers.[135] Typically, frameworks (e.g., MOFs) are porous materials with modular architectures of metal nodes and organic linkers, impacting the band structure by inducing higher charge localization.[124] It is supported by spatial separation of linkers in the scaffold of the framework or as embedded guest molecules, which promote localization of electronic states rather than a delocalization within a conduction band (see the differences in potential energy surfaces (PES) in Figure 8). Band-like transport should be even less expected for photoswitchable framework materials with photoswitches incorporated into the framework scaffold since the switching response is related to rather strong structural changes by chromophores, inducing higher disorder and lattice vibrations, increasing charge localization. Thus, the hopping mechanism with electron (or hole) hops between localized states is a dominant pathway for charge carrier transport in this case (as depicted in Figure 8b). It requires overcoming the activation energy, permitting the move from one localized site to another. It depends on the energy gap difference between localized states and the reorganization energy, $\lambda$, needed to reorganize the molecular or lattice environment (e.g., vibrational modes) for transfer. The process can be illustrated as parabolic PES representing the initial (*i*) and final (*f*) states with reorganization energy corresponding to the vertical transition energy between the two PES and the crossing point related to the probability for electron transfer. Here, the strength of the spatial interaction, for example, electronic coupling ($J$) between the hopping sites, approximately reflected by spatial overlap of molecular orbitals, is particularly relevant for the electron hopping rate. A stronger coupling indicates that the transition is more likely to occur when it reaches the intersection. In the weak coupling regime, when electron transfer is slower than nuclear motions, the electron "hops" between localized sites (i.e., donor and acceptor) after nuclear reorganization, and the CT rate depends quadratically on the coupling. This concept is known to be used in the Marcus theory of charge transfer, which is most often applied for hopping in frameworks.[72] However, several theories are generally used to describe hopping transport.[136,137] Since different initial and final states may be involved in CT via hopping, in this manuscript, we focus mostly on photoswitching electron conduction induced by photoactive molecules (i.e., not the metal nodes present in MOFs), therefore, diverse through-space scenarios are discussed below.

As mentioned in the previous section, the first proof of concept for photoswitching of electron conduction in framework materials was realized by us in 2018 for UiO-67 with nitro-substituted SP (see **Figure 9**a) as a guest molecule.[53] A stable structure with a high switching yield under 70% conversion to MC upon UV irradiation was confirmed. Conductivity measurements showed values of $4.1 \times 10^{-9}$ S $m^{-1}$ for the SP loaded MOF and $4.1 \times 10^{-8}$ S $m^{-1}$ after the conversion to the MC form. The reversibility of

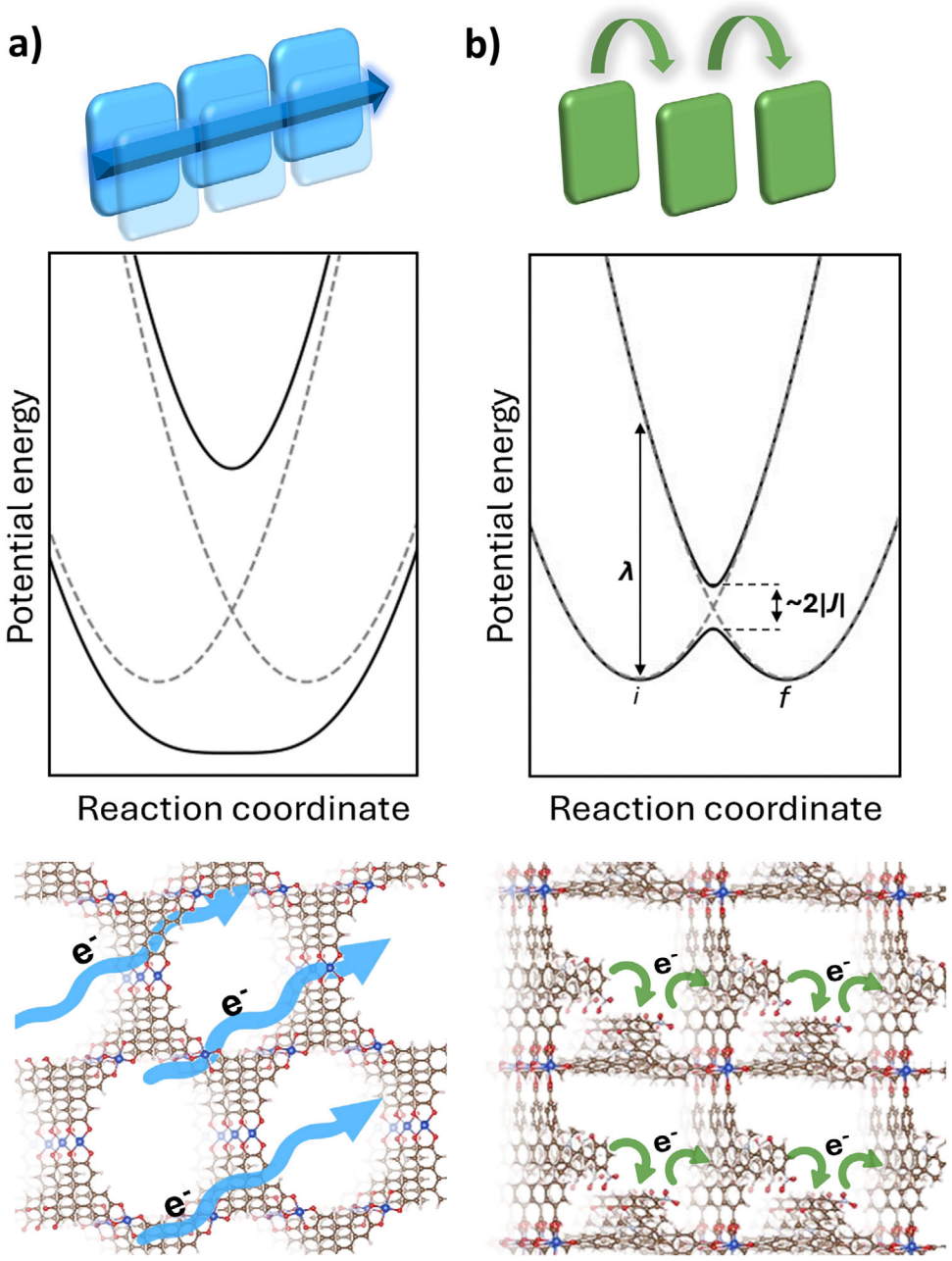


**Figure 8.** The schematic visualization of a a) band-like and b) charge hopping-based electron transfer mechanisms. Left panel: Barrierless movement of delocalized charge carriers occurs in adiabatic, strong electronic coupling regime (solid curves), where charge carriers are delocalized over many sites and move coherently through extended electronic states (visualized with blue arrows). Such transport was reported for $Cu_3(HHTP)_2$ monolayers exhibiting a unit cell with $D_{6h}$ symmetry and in specific experimental conditions.[135] Right panel: Electron hopping between the diabatic potential energy surfaces (dashed lines) of the initial and final localized sites is illustrated on the right. The microscopic parameters that define the CT rate in the weak coupling regime are shown for clarity, with further explanation provided in the text. The energy difference between the hopping sites is neglected in this scheme. Green arrows schematically indicate electron hops within the MOF material.

the reaction was demonstrated by several switching cycles, with a minor 5% loss in effect due to photodegradation. The conductivity modulation with light was proved to result from SP-to-MC conversion because of significant differences in the electronic structure of guest molecules, their molecular length and electronic coupling between neighboring sites providing hopping states permitting charge carrier transport within the material. Here, MC was shown to have more pronounced electron delocalization in frontier orbitals, for example, highest occupied molecular orbital (HOMO), as depicted in Figure 9a. Together with the structure elongation upon bond breaking, it allowed smaller distances between the hopping sites and better electronic coupling, increasing the CT rate. In Figure 9a (on the right), the values of the electronic coupling between neighboring SP and MC

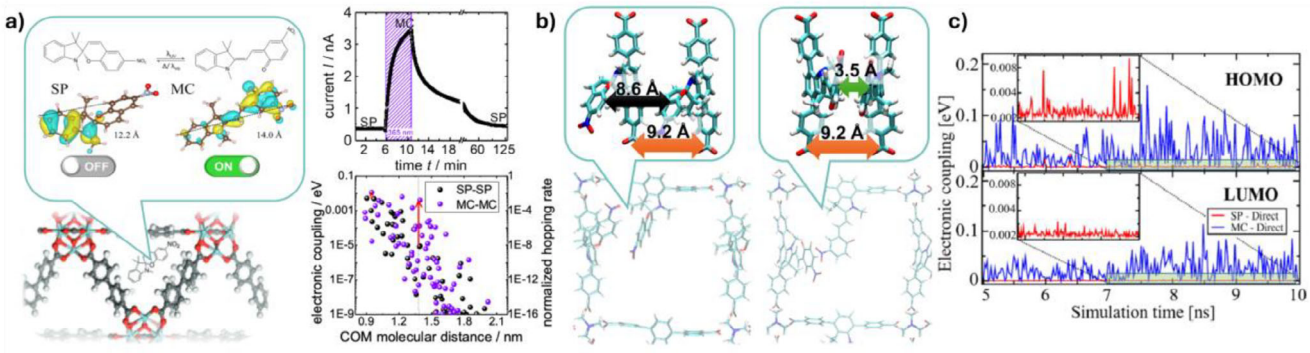


**Figure 9.** a) Representation of photoswitching of electron conduction in UiO-67 with embedded SP in the pores. (Top right) The increase in current upon SP-MC photoisomerization in SP-loaded UiO-67. (Bottom right) Electronic coupling between SP species (SP-SP) and MC species (MC-MC) in MOF pores as a function of their center of mass distance. b) Computational model of SP-based MOFs with SP incorporated into a paddle-wheel SURMOF scaffold with interlayer distances ≈9.2 Å regulated by the dabco pillar linkers. Upon photoisomerization, structural rearrangements of linkers in room temperature trigger the decrease of intermolecular distances between neighboring linkers from 8.6 Å (in SP form) to ≈3.5 Å (in MC form), permitting $\pi$–$\pi$ interactions and better electronic coupling, enhancing hopping transport. c) Time evolution of the electronic coupling between HOMO and LUMO orbitals of SP-linkers (red) and MC-linkers (blue) in Cu2(SP)2(dabco) and Cu2(MC)2(dabco) MOFs. Figure a) (right) adapted with permission from ref. [53] Copyright, 2018. Published by John Wiley and Sons. Figures b) and c) with permission from ref. [72] Copyright 2023. Published by Springer Nature.

molecules calculated using density functional theory (DFT) are provided. They indicate lower couplings between SP molecules than MC molecules (16 times), which change significantly with the increase of the hopping distance. Specifically, on distances ≈14 Å, the on/off ratio between more conductive (MC) and less conductive (SP) photoswitches reaches even four orders of magnitude. This observation suggested that optimizing the distances between photoswitches and their orientations in a material can give huge on/off ratios, and thus, significant changes in the electron conduction controlled by light.

Since one of the best ways to control chromophores in frameworks is to incorporate them in the scaffold and manipulate them with linker lengths or framework topologies, in silico models for SP-based MOFs were developed by Mostaghimi et al.[72] (see an example in Figure 9b). Several types of SP- and MC-based layer linkers were used for MOF models to understand the impact of different functional groups on electronic coupling between the molecules. Dabco and bipyridine were implemented as pillar linkers to mimic different interlayer distances in the SURMOF (i.e., 9.2 Å and 13.7 Å), which impact molecular separation between the photoswitches, thus the spatial overlap of their molecular orbitals deciding about the strength of the electronic coupling. Sampling of structural motions of modeled MOF structures by performing molecular dynamics simulations at room temperature revealed that layer linkers in SP-based MOFs possess completely different structural motions and flexibility of linkers. It significantly impacted attained interaction sites and the possibility of a CT. SP-to-MC photoisomerization (assumed in the model to be 100%) permitted the formation of structurally more flexible MC molecules, which allowed the intermolecular distance decrease between MOF linkers from 8.6 Å (in SP-based MOFs) to 3.5 Å (in MC-based MOFs), see Figure 9b. It should be noted that the interlayer distance in this case was still the same, because the same dabco pillar was explicitly modeled. Such a huge change in the distances between photoswitches leads to different strengths of the electronic coupling (see Figure 9c), which was strongly enhanced in the case of the MC-based MOF due to the presence of $\pi$–$\pi$ interactions, as well as superexchange-like (through-space) electronic coupling. This was additionally allowed by the $\pi$-electron delocalization of MC. The authors pointed out that dynamic disorder in such systems plays an important role, directly impacting the electron hopping rates and electron conduction of materials. The electronic coupling values in MC-based MOFs were shown to be 23 times higher than in the SP case, demonstrating an on/off photoswitching ratio of ≈500 for hole charge carrier transport.

DAE photoswitches incorporated in frameworks were reported permit the modulation of electron conduction by Yu et al.[105] and Dolgopolova et al.[117] As depicted in Figure 3b, Yu et al. studied COFs with a DAE-based photoswitchable linker (1,2-bis(5-formyl-2-methylthien-3-yl)cyclopentene) covalently integrated into the framework, while Dolgopolova et al. implemented DAE and SP in MOFs as main backbone linker and attached to the MOF linker, respectively. The on-off ratio triggered by reversible photoisomerization was 200 in COFs with conductivity values of $1 \times 10^{-5}$ S $m^{-1}$ (open ring under visible light) and $2 \times 10^{-3}$ S $m^{-1}$ (closed ring under UV light). The authors reported that photoinduced switching enhanced conductivity due to $\pi$-conjugation extension through photocyclization reaction. They confirmed that the ring-closing/opening reactions did not compromise the integrity of the frameworks since the formation of covalent bonds between methylthiophene units is known to occur in one plane. Using DFT calculations, they denoted the decrease of the band gap from 1.606 eV for COF-O to 0.543 eV for COF-C, as well as differences in the density of states of both materials. They have not explicitly discussed the charge transport mechanism in both materials but suggested that due to the 2D layered structure of the COF, it likely occurs in-plane along the framework, with potential contributions from interlayer $\pi$-$\pi$ interactions facilitating through-space hopping. Since the interlayer distance decreased from 6.6 Å (in COF-O) to 6.3 Å (in COF-C), the role of stacking interactions changes. However, the photoinduced conversion triggers bond formation within COF layers, that is, modulation of through-bond pathways may be more significant.

A similar observation for the conductivity enhancement attributed to changes in $\pi$-conjugation length after photocyclization was reported in MOFs by Dolgopolova et al.[117] The average conductivity values for the non-irradiated samples of the DAE-based MOFs: $Zn_2(BPDC)_2(BPMTC)$ and $Zn_2(SDC)_2(BPMTC)$ with Zn-based paddle-wheel units connected by $BPDC^{2-}$ ($H_2BPDC$ = biphenyl-4,4′-dicarboxylic acid) or $SDC^{2-}$ ($H_2SDC$ = stilbene-4,4′-dicarboxylic) with the photochromic DAE-based axially coordinated to the nodes, were found to be $6.4 \times 10^{-5}$ and $9.5 \times 10^{-5}$ S m$^{-1}$. However, after UV exposure approximately three times conductivity enhancement was detected, resulting in conductivity of $1.7 \times 10^{-4}$ and $2.9 \times 10^{-4}$ S m$^{-1}$, respectively, measured using two-contact probe pressed-pellet setup on bulk MOFs. In addition, using a different secondary building unit (Zr-based) and slightly modified $H_2BCMTC$ linker another MOF could be obtained with a higher conductivity of $1.4 \times 10^{-3}$ S m$^{-1}$ before UV and $2.3 \times 10^{-3}$ S m$^{-1}$ after UV, resulting in an on/off ratio of 1.64. The authors also integrated SP units into MOF frameworks by attaching them to the linker to investigate photoswitched conductivity enhancement. Specifically, they synthesized the $Zn_2(DBTD)(TNDS)$ MOF was synthesized ($H_4DBTD$ = 3′,6′-dibromo-4′,5′-bis(4-carboxyphenyl)-1[1,1′:2′,1″-tetraphenyl]-4,4′′-dicarboxylic acid, TNDS = 1′,3′,3′-trimethyl-6-nitro-4′,7′-di(pyridin-4-yl)spiro[chromene-2,2′-indoline]). They demonstrated that the SP-MC conversion upon irradiation was possible without framework degradation even after several consecutive irradiation cycles. However, the conduction measurements for SP-based MOFs were limited due to fast cycloreversion kinetics, preventing precise conductivity measurements. Thus, they reported a relative increase in conductivity upon UV irradiation of 1.2 times. Finally, it was stated that in a SP-based MOF, UV-induced photoisomerization of SP to MC allowed the formation of a charge-separated merocyanine form, increasing frontier orbitals delocalization and decreasing spatial separation. As discussed for similar molecules above, this facilitates charge hopping, promoting conductivity enhancement.

Recently, Liu et al. presented a series of conductive MOFs thin films where the electron conductivity was reversibly remote controlled by light.[12] For that, SURMOF films based on $Cu_3(HHTP)_2$ MOF ($Cu_3$(2,3,6,7,10,11-hexahydroxytriphenylene)$_2$), which is known to be intrinsically conductive, were prepared. The conductivity of the pristine $Cu_3(HHTP)_2$ was reported to be 4.13 S m$^{-1}$ and exact conduction mechanism in this MOF remains under debate in the literature with the tendency to the band-like mechanism. However, a more recent study has reported metallic behavior.[135] The films were loaded with AB, DAE, SP, and hexaarylbiimidazole (HABI)[138,139] as guest molecules in the pores (see **Figure 10a**). Upon guest loading, a slight reduction in conductivity was observed, with the photoswitch@$Cu_3(HHTP)_2$ conductivities (measured by 2-probe DC) ranging ≈3.90 S m$^{-1}$. HABI@$Cu_3(HHTP)_2$ exhibited the highest conductivity of 3.75 S m$^{-1}$. Based on DFT calculations, the decrease in the density of states near the Fermi level was detected. Since this change is differently modulated after the photoconversion of photoswitches, different on/off ratios were observed with the most significant reversibly modulated electron conduction by up to 15% for HABI (Figure 10b). Cycling experiments demonstrated reversible conductivity switching over at least three cycles, with no evidence of photodegradation under the reported conditions. Moreover, the spectroscopic analysis of the UV–vis absorption spectra confirmed that light-induced isomerization of the photoswitches in the $Cu_3(HHTP)_2$ MOF pores were similar to the isomerization in solution with photoconversion in MOF pores similar to other studies reported, that is, approximately 65% for AB, 60% for DAE, 70% for SP and 84% for HABI. Finally, the authors used the HABI@$Cu_3(HHTP)_2$ SURMOF film for exploring its sensor performance for exposure of volatile organic compounds such as ethanol, 1-propanol, toluene, and water. By measuring the change in current at a constant DC voltage of +1 V, enhancements in selectivity were reported: 63% for 1-propanol, 43% for toluene, 35% for ethanol, and 16% for water in the UV-induced radical state of HABI compared to its dimer state. Moreover, by photoswitching the sensor to different states, the sensitivity and selectivity of such a sensor array became more diverse and, thus, the accuracy of identifying different analytes enhanced. Previously, some of the authors termed it as photoprogrammable sensors.[140] Here, the accuracy of identifying the above-mentioned analytes at various concentration enhanced from 84% to 99%.[12]

A similar light-induced electron conductivity principle was realized in 2D COF BDFamide-Tp with SP-based guest molecules.[104] However, the pristine COF was found to be insulating, showing low current below 0.1 nA, which was explained to originate from the $\beta$-ketoenamine type linkage, breaking the conjugation between the benzodifuran units, hindering the band-like CT in the conjugation in the 2D layer. When the organic semiconductor DPP4T was deposited on top of BDFamide-Tp (see Figure 10c), the conductivity of the material increased by three orders of magnitude. The effect was attributed to an interfacial doping, because the p-type semiconductor DPP4T can transfer electrons to the electron-deficient BDFamide-Tp, permitting the generation of the hole charge carriers. The photoswitching of conduction of this device could be realized only after the encapsulation of SP into the pores of the COF, which differently modulated the measured electronic responses upon the light-driven MC formation. The domination of MC triggered the decrease of conductivity, while the opposite effect was measured for SP (see Figure 10d). Thus, the device became photoswitchable with the current on/off ratio after UV versus vis illumination of 100. However, the exact reasoning for conductivity photoswitching changes was not provided.

Finally, in the recent manuscript by Li et al.[120] a novel approach, based on photoswitching and manipulation with conductive states, capable of processing information on the molecular level was reported. Using a SURMOF $Cu_2(F_2AzoBDC)_2$(dabco) (Figure 2) with *ortho*-fluorinated azobenzene molecules as layer linkers organized in a periodic array, a domino-toppling-like directional transport of an electron was realized (see **Figure 11**).

Here, instead of being modulated only by light, the charge transport in the material was also manipulated by applying an electric field. Upon the photoexcitation of AB from its *trans* to *cis* state by irradiation with green light of 530 nm (see step 1 in Figure 11), the thermal back isomerization

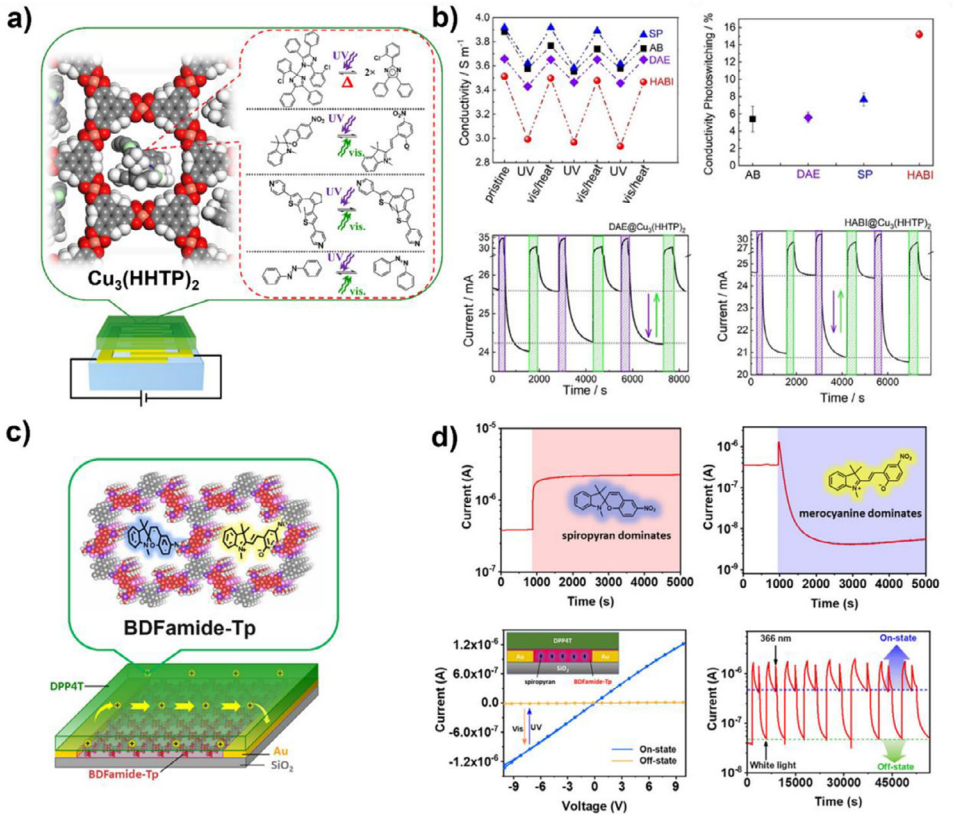


**Figure 10.** Photoswitching of conduction in 2D frameworks: a) $Cu_3(HHTP)_2$ SURMOF film on interdigitated gold electrodes with embedded photochromic HABI molecules, and the illustration of other photoswitches used in the study, that is, SP, DAE, and AB. The summary of corresponding photoisomerization processes is given for clarity. b) Conductivity changes over three consecutive switching cycles in $Cu_3(HHTP)_2$ SURMOFs loaded with AB, DAE, SP, and HABI with the respective change of conductivity phoswitching and current response under repeated light switching at +1 V. Violet sections represent UV light irradiation and the green sections represent visible light irradiation or thermal relaxation. c) Schematic representation of the thin-film device with DFamide-Tp COF encapsulated with SP underneath DPP4T polymer with DFamide-Tp/DPP4T as an active layer. d) (Upper panel) Dynamic current response during the switch-on process under visible light (pink zone, SP form) in comparison to the switch-off process under UV light (purple zone, MC form). (Bottom left) I–V curves of a photoswitchable device after 8 min of UV illumination (yellow, off-state) or 6 min of vis illumination (blue, on-state). The inset shows the device configuration. (Bottom right) Switching cycles of the electron conduction photoresponse enabled by DFamide-Tp COF encapsulated with SP. Figures a) and b) adapted with permission from ref. [12] Copyright, 2025. Published by John Wiley and Sons. Figures c) and d) adapted with permission from ref. [104] Copyright, 2022. Published by American Chemical Society.

was accelerated by applying an electric field (see step 2 in Figure 11). The injected electrons change the neutral *cis* form to a $cis^{\bullet-}$ radical anion, but due to the low energy barrier, the $cis^{\bullet-}$ state quickly changes back to $trans^{\bullet-}$, allowing the electron to hop to the next neutral *cis*. The process is repeated, creating a domino-like chain reaction of isomerization and electron hopping. When the light initiating the first step is switched off, the current applied between the ITO bottom electrode with the grown SURMOF and the gold top electrode decreases back to the base current within a time constant of ≈10 min. Since this switching process can be repeated and interpreted as writing and storing information upon green light irradiation (with metastable *cis* formation) and reading or erasing information upon electron injection, such materials can be used for photoswitchable optoelectronic information storage and self-erasing readout. By further tailoring the framework composition and the electronic structure of its components, new advanced functional materials and their quantum-level electronic control could be realized in the future.

### 3.4. Framework Guided Conductivity

In this section, we aimed to summarize the conduction photoswitching properties of reported framework materials. As we demonstrated, photoswitchable proton conduction in framework materials has proven to be effective in membranes,[5,7] and thin films,[94] especially under high humidity conditions (>90% RH) and elevated temperatures (>300 K), demonstrating minimal photodegradation over multiple cycles (see **Table 1**). It is particularly relevant for applications where efficient and clean electric energy production by proton-exchange membrane fuel cells is needed or in chemical sensors.[6,141] Among protic species, water consistently leads to higher on/off switching ratios compared to anhydrous environments due to its high propensity for the

**Table 1.** Summary of the reported conductivity values measured in photoswitchable framework materials.

| Framework material | Photoswitch | Incorporation | Specific conditions | Σ [S $m^{-1}$] | Type | Mechanism | On/off ratio | Refs. |
|---|---|---|---|---|---|---|---|---|
| **SURMOF** $Cu_2(F_2AzoBDC)_2(dabco)$ | o-fluoroazobenzene | Attached to the linker | 25 °C, anhydrous conditions | Butanediol: $9.0 \times 10^{-6}$ (*trans*), $6.1 \times 10^{-6}$ (*cis*) Triazole: $1.2 \times 10^{-4}$ (*trans*), $7.9 \times 10^{-5}$ (*cis*) | $H^+$ | N/A | Butanediol: 1.48 Triazole: 1.52 | [54] |
| **SURMOF** $Cu_2(SP\text{-}BPDC)_2(dabco)$ | SP | Attached to the linker | 25 °C, Water (93% RH), MeOH, | Water: $2.5 \times 10^{-6}$ (SP), $3 \times 10^{-8}$ (MC) MeOH: $1 \times 10^{-7}$ (SP), $5 \times 10^{-9}$ (MC) EtOH: $7 \times 10^{-8}$ (SP), $2 \times 10^{-9}$ (MC) | $H^+$ | Grotthuss-like | Water: 82 MeOH: 20 EtOH: 35 | [94] |
| **ZIF-8 Membrane** SSP@ZIF-8 | SSP | Guest | At 75 and 25 °C, 95% RH, 10%SSP | 75 °C: $1.8 \times 10^{-4}$ (SP), 5.0 (MC) 25 °C: $3.1 \times 10^{-5}$ (SP), $1.0 \times 10^{-2}$ (MC) | $H^+$ | Mixed (Grotthuss + vehicle) | 75 °C: $2.8 \times 10^4$ 25 °C: ≈300 | [7] |
| **MOF Membrane** PSS–SSP@Cu-TCPP | SSP | Guest | 55 °C and 95% RH | $1.37 \times 10^{-2}$ (MC), $1.29 \times 10^{-5}$ (SP) | $H^+$ | Mixed (Grotthuss + vehicle | 1068 | [5] |
| **COF** COF-HNU9 | DASA | Attached to the linker (dangling groups) | 98% RH, 25 °C, 80 °C | 25 °C: $5.62 \times 10^{-3}$ (Open-ring), $3.74 \times 10^{-1}$ (Closed-ring) 80 °C: 2.0 (Closed-ring) | $H^+$ | Grotthuss | 25 °C: 66 80 °C: N/A | [6] |
| **ZIF Membranes** SSP@ZIF-8 | SSP | Guest | 25 °C, 0.5 M LiCl aqueous solution | $1.6 \times 10^{-2}$ (MC), $7.1 \times 10^{-4}$ (SP) | $Li^+$ | Hopping | 23 | [118] |

(*Continued*)

**Table 1.** (Continued)

| Framework material | Photoswitch | Incorporation | Specific conditions | Σ [S m$^{-1}$] | Type | Mechanism | On/off ratio | Refs. |
|---|---|---|---|---|---|---|---|---|
| **MOF thin film** | azobispyridine | Backbone linker | ≈25 °C | (1): $3.2 \times 10^{-3}$ (Dark), $1.65 \times 10^{-2}$ (Light). | Electron | Hopping | (1): 5 | [116] |
| (**1**): Cd(azbpy)(suc) | | | | (2): $2.64 \times 10^{-3}$ (Dark), $9.76 \times 10^{-3}$ (Light). | | | (2): 3.7 | |
| (**2**): Cd(azbpy)(msuc) | | | | (3): $1.29 \times 10^{-3}$ (Dark), $3.61 \times 10^{-3}$ (Light). | | | (3): 2.8 | |
| (**3**): Cd(azbpy)(mglu) | | | | (4): $2.07 \times 10^{-3}$ (Dark), $6.60 \times 10^{-3}$ (Light). | | | (4): 3.2 | |
| (**4**): Cd(azbpy)(glu) | | | | | | | | |
| **MOF film** | SP | Guest | Ar atmosphere | $4.1 \times 10^{-9}$ (SP), $4.1 \times 10^{-8}$ (MC) | Electron | Hopping | 10 | [53] |
| SP@UiO-67 | | | | | | | | |
| **MOF** | SP | Attached to the linker | ≈25 °C | N/A | Electron | Hopping | 1.2 | [117] |
| $Zn_2$(DBTD)(TNDS) | | | | | | | | |
| **MOF** | DAE | Backbone linker | ≈25 °C | (2): $6.4 \times 10^{-5}$ (Open-ring) $1.7 \times 10^{-4}$ (Closed-ring) | Electron | Hopping | (2): 2.6 | [117] |
| (**2**) $Zn_2$(BPDC)$_2$(BPMTC), (**2′**) $Zn_2$(SDC)$_2$(BPMTC, | | | | (2′): $9.5 \times 10^{-5}$ (Open-ring) $2.9 \times 10^{-4}$ (Closed-ring) | | | | |
| (**3**) ($Zr_6$($Me_2$BPDC)$_4$(BCMTC)) | | | | (3): $1.4 \times 10^{-3}$ (Open-ring) $2.3 \times 10^{-3}$ (Closed-ring) | | | | |
| **COF** | DAE | Backbone linker | ≈25 °C | $1 \times 10^{-5}$ (Open-ring), $2 \times 10^{-3}$ (Closed-ring) | Electron | Hopping | 200 | [105] |
| **SURMOF** | AB | Guest | ≈25 °C | $Cu_3$(HHTP)$_2$: 4.13 | Electron | Band-like[a]: $Cu_3$(HHTP)$_2$ | AB: 5.4% | [12] |
| AB@$Cu_3$(HHTP)$_2$ | DAE | | | Photoswitch@$Cu_3$(HHTP)$_2$: ≈3.0–4.0 | | N/A: AB@$Cu_3$(HHTP)$_2$ | DAE: 5.6% | |
| DAE@$Cu_3$(HHTP)$_2$ | SP | | | HABI@$Cu_3$(HHTP)$_2$: 3.75 | | DAE@$Cu_3$(HHTP)$_2$ | SP: 7.7% | |
| SP@$Cu_3$(HHTP)$_2$ | HABI | | | | | SP@$Cu_3$(HHTP)$_2$ | HABI: 15.2% | |
| HABI@$Cu_3$(HHTP)$_2$ | | | | | | HABI@$Cu_3$(HHTP)$_2$ | | |

[a] Conduction mechanism is not unambiguously deciphered, but many theoretical investigations indicate a band-like charge transport.

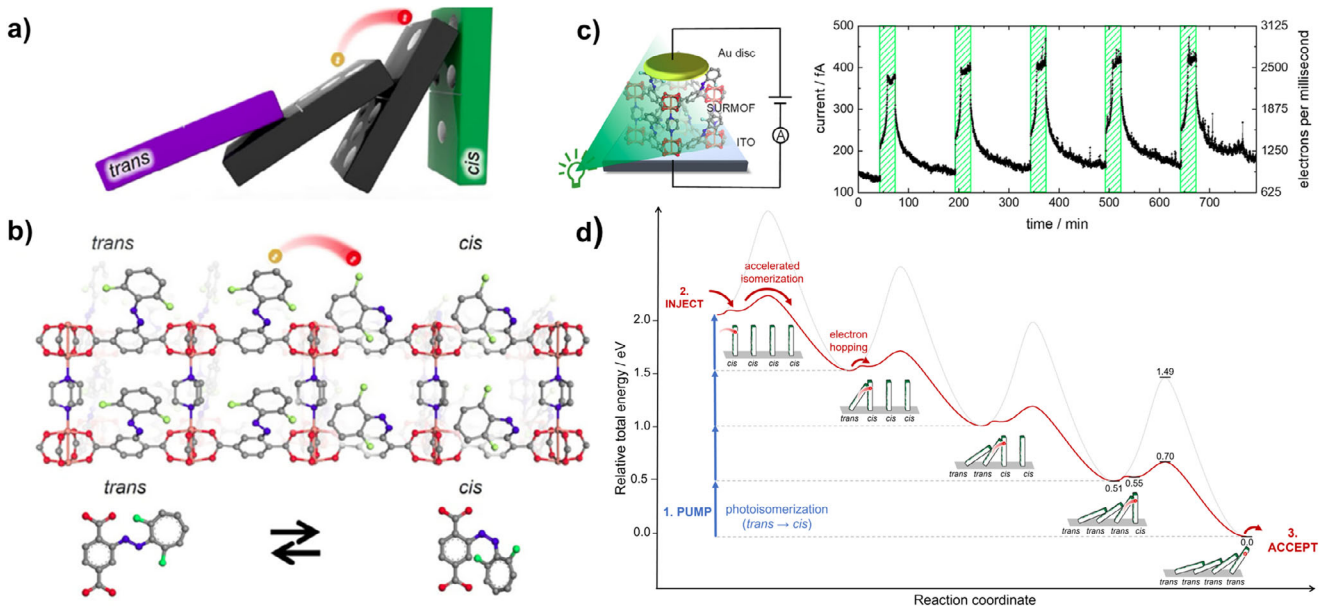


**Figure 11.** Mechanism of a light-pumped domino-toppling-like directional transport of an electron in $Cu_2(F_2AzoBDC)_2(dabco)$ SURMOF material. a) Domino analogy: electron transfer (red sphere) triggers sequential toppling of upright dominoes (meta-stable *cis* isomers) into lying ones (*trans* isomers). b) Schematic representation of *cis* to *trans* isomerization in the SURMOF structure. c) Current response under repeated green-light irradiation (530 nm, 30 min) with ITO and Au electrodes at 1 V bias. d) Mechanism of electron propagation via light-induced initial *trans* to *cis* isomerization ("pumping"), followed by directional *cis* to *trans* switching coupled with electron transfer to the neighboring *cis* isomer to carry on the chain reaction resetting the system to the all-*trans* state. Adapted with permission from ref. [120] Copyright, 2025. Published by John Wiley and Sons.

formation of hydrogen-bond networks that facilitate hopping of the proton. Conductivity values for such a conduction range between $\approx 10^{-9}$ and 5.0 S $m^{-1}$ (see Table 1) with the highest conductivity observed in a membrane system SSP@ZIF-8 with MC embedded as a guest molecule at 75 °C and 95% RH. Therefore, such frameworks have potential for advanced chemical sensing applications, fuel cells, and bio-electronic devices, as well as for photoswitchable devices such as proton conducting field-effect transistors,[7] and, as recently demonstrated, for applications in photo-programmable sensors for environmental monitoring.[12]

While Grotthuss-type mechanism is commonly used to explain the $H^+$-transport in these systems, several studies[7,9] have also reported mixed behavior influenced by framework confinement and water content. The interpretation of conduction mechanisms remains complex, as high activation energies (>0.4 eV) can result not only from the vehicle transport but also from steric hindrance. These findings show the importance and the need for further investigations for better understanding of proton transport pathways and exploration of alternative framework materials to achieve higher conductivities with enhanced switching performance.

From the analysis of state-of-the-art, we can summarize that photoswitching of electron conduction in framework materials has been reported predominantly for MOFs owing to their greater structural tunability and ability to incorporate photoswitches in desired conditions. The conductivity values in the photoswitchable MOF materials range from $\approx 10^{-9}$ to $\approx 3.0$ S $m^{-1}$ (see Table 1) with the highest values characteristic to intrinsic high conductivities of pristine frameworks, for example, $Cu_3(HHTP)_2$ SURMOFs. It permits the realization of light-programmable sensors and other smart electronic devices, however, there is a scarce number of other MOF framework materials resulting in such high conductivities that can be photoswitched. (The detailed analysis of other photoswitchable materials with switchable electronic conduction properties in comparison to this MOF was provided in Table S1, Supporting Information in ref. [12]) Typically, MOFs exhibit low intrinsic electron conductivity due to their porous and sometimes insulating architectures, thus incorporation of photoswitches in some cases create new conductive pathways, increasing conductivities or due to specific interactions disrupt conductive pathways, allowing light-controlled modulation of responses. However, the presence of photoswitchable molecules in frameworks either as linkers or guest molecules is required for such a response to take place.

In general, reversible changes (i.e., the on/off effect) in electron conductivity due to photoswitching in MOF frameworks were calculated to range typically from one to two orders of magnitude, related to the change in intermolecular distances and dynamics in materials, as well as orbital overlap or mixing in the density of states. Experimentally reported on/off ratios are lower (see Table 1), which may be partially due to the lower photoconversion probabilities known for photoswitches than assumed in theoretical models. In addition, subtle differences in the nanostructure may result in deviations. In most cases, electron hopping regulates charge transport in reported materials with some exceptions to systems with strong conjugation as in $\pi$-stacked systems, that is, $Cu_3(HHTP)_2$ MOF.

COFs have demonstrated photoswitching primarily through modulation of $\pi$-conjugation in photochromic linkers, though the number of reported examples remains limited and conductivity values are generally lower. However, the on/off

ratio for electron conduction photoswitching was reported to be rather high, that is, 200 (see Table 1). COFs present advantages over MOFs for specific applications such as microelectrochemical energy storage and flexible electronics, where their covalent bonding network offers better mechanical stability during cycling and avoids the heavy metal related limitations of MOFs.[142]

From our analysis, there is virtually none for ZIFs reported for photoswitched electron conduction, but these materials are known for proton conduction photoswitching. This is likely due to the structural characteristics of ZIFs and lack of extended $\pi$-conjugation in imidazolate-based frameworks, making them less suitable for electron conduction.

The summary of findings suggests that MOFs currently offer the most versatile platform for integrating dynamic light-induced electron conduction into porous framework materials, while COFs represent an emerging direction and ZIFs or other framework materials remain largely unexplored for this functionality. Altogether, it opens the vast variety of further possibilities toward advancing functionality of materials,[143–145] starting from engineering the composition of frameworks[132–134] (e.g., by metal node engineering and linker design) or heterojunction-like interfaces up to post-synthetic doping, hybrid architectures of MOF-COF composites, MOF-graphene hybrids, or MOF-perovskite hybrids, as well as structures with designed donor-acceptor domains allowing for efficient charge carrier separation and transport.

## 4. Challenges and Perspectives

Despite exciting progress in the development of frameworks with photoswitchable conduction, several challenges limit the fabrication of a wide range of new photoswitchable framework materials, currently hindering the realization of their full potential in practical applications.

**Optimization of Photoswitchable Molecules:** First, the number of photoswitchable molecules that can operate under the desired experimental conditions is still rather small as the requirements on their performance related to quantum efficiency and fatigue resistance limit the number of useful candidates. In addition, optimizing the excitation wavelengths of photoswitches toward longer wavelengths is important for overcoming the light penetration depth limitation, which affects the number of molecules efficiently photoactivated within the material. Combined with wavelength-orthogonal design of photoswitches to achieve selective absorption by the reverse isomer, this would allow higher probabilities of conduction with a better controlled isomer competition.

**Control Over Competing Processes:** Going in line with summaries provided in previous sections, photoconversion of photoswitches in frameworks, lifetimes of photoactive states, their stability and photodegradation impact the quality of functional materials and cycling performance. Modulating responses through environmental tuning of the electronic structure of photoswitches or by introducing additional molecules or forces to suppress undesired processes may represent an important pathway toward practical implementation. It is particularly relevant for photoswitches since the light-induced changes of their physicochemical properties are highly sensitive to various environmental factors. In addition, the electron and proton conduction types are based on subtle electronic effects and intermolecular interactions, which are sensitive to the quality of the material, therefore, the presence of side reactions or defects disrupts measured responses, decreasing their performance and reversibility. A better control and tuning of competing processes is essential for the functionality of framework materials. Nevertheless, the research field remains in its early stages when it comes to understanding the photochemical and photophysical phenomena occurring within materials under experimental conditions. Consequently, the development of robust computational methods and comprehensive experimental characterization are critical as foundational efforts.

**Integration of Photoswitches and Synthesizability of Frameworks:** The mode of photoswitch incorporation (e.g., as guest, backbone linker, or side group) significantly influences conduction behavior. Backbone integration may hinder isomerization, especially for switches undergoing large structural rearrangements, while pore loading is more feasible but often limited by steric hindrance, requiring large pore sizes. Covalent attachment as side groups allows ordered placement, however it may complicate synthesis. Synthesizability of frameworks and design of experimental conditions toward structure-controlled synthesis create a promising direction aiding to overcome this challenge.[146] However, reliable tools designed for specific experiments and types of framework materials using automated systems (self-driving labs) and artificial intelligence are presently still in development.[147]

**Scaling of Synthetic Platforms:** Another significant challenge of photoswitched materials (even beyond frameworks) is the poor light penetration in bulk materials addressed above. Since photoisomerization often remains confined to the surface, preventing switching throughout the structure, special forms of materials are more efficient than others. Membranes and thin films have shown to be a good alternative to this limitation, but such materials require specific experimental techniques and conditions,. Standardization and adaptation of synthetic methods permitting accessibility of efficient techniques and automatization of processes could help in large-scale data acquisition for structure-property relationships of frameworks with data-driven and knowledge-driven design of improved materials.

**Design of New Architectures and Hybrid Systems**: Finally, proton conductivity of frameworks is rather moderate and permits improvements by modifications of photoswitches or tuning framework topology, since this type of conduction is strongly related to hydrogen-bonded networks and properties of guest molecules. However, electron conductivities of frameworks are typically low and are improved by $\pi$-conjugated and well-stacked architectures that facilitate efficient charge transport, but there are not many such materials currently available, where the photoswitching generates currents necessary for practical applications. Addressing this issue requires designing materials where local photoisomerization events translate into amplified, long-range changes in transport properties, such as through pore gating, cooperative network rearrangements, or phase transitions. Moreover, framework

structures with designed donor-acceptor domains or heterojunction-like interfaces containing different molecular moieties allowing for efficient charge carrier separation and transport offer an interesting pathway for the development of improved systems. A wide scientific community is engaged in new developments with this respect; thus, we envision noticeable progress in this direction soon. In addition to ongoing developments in electronic structure methods and multiscale modeling techniques, deeper understanding of conduction mechanisms will be possible, and combined with design strategies, automated tools and experiment-theory feedback loops will permit emergence of new framework materials with advanced functionalities.

## 5. Conclusion

Photoswitching of electron, proton and other ionic conductivities offers a powerful strategy to remotely and reversibly control properties of materials using light. Such functionality permits a huge variety of possible applications, including optical memory devices, reconfigurable electronics, neuromorphic systems, artificial proton pumps, smart batteries, or light-tunable membranes. Reversibility of responses is provided by photoactive molecular switches that reversibly change their structure and electronic properties under light. Efficient photoconversion of photoswitches can be realized in framework materials, which offer a wide range of tunable functionalities, as well as modular architecture and porous structure. Thus, integration of photoswitches into frameworks permitted light-controlled gas sorption or release, catalysis, or sensing. The difference in response induced by light is connected to the fact that electronic properties of photoisomers and their reactivity change upon light exposure, resulting in differences in interactions with other species, binding in the pores or even modulating charge transport pathways of conductive frameworks or inducing conductivities of initially nonconductive materials. In this review, we have highlighted strategies applied toward photoswitching of electron and proton conduction pathways using molecular switches incorporated in MOFs, COFs, ZIFs, and other framework materials as guest molecules and scaffold components, introduced either by direct synthesis from functionalized linkers or after PSM. We explained the differences in conduction mechanisms, as well as microscopic parameters and phenomena modulating the on/off switching of conduction. We demonstrated frameworks with light-responsive proton conduction, offering potential for applications in smart membranes, sensors, and energy devices. Since materials that combine good electron conductivity with photoresponsive properties are still under development, and the first evidence of such possibilities was only recently reported, we have highlighted the significant potential of frameworks for diverse smart materials. In view of their enormous potential, we are convinced that these materials will have a bright future in fields ranging from energy and sensing to soft robotics and bioelectronics.

## Acknowledgements

This research was funded by the Deutsche Forschungsgemeinschaft (DFG) via SPP 1928 COORNETs (HE7036/6 and WE1863/37) and via GRK 2450 "Scale bridging methods of computational nanoscience." H.P.H. acknowledges funding by the Deutscher Akademischer Austauschdienst (DAAD). S.H. thanks the Einstein Foundation Berlin as well as Humboldt University for generous support. We acknowledge support by the KIT-Publication Fund of the Karlsruhe Institute of Technology.

Open access funding enabled and organized by Projekt DEAL.

## Conflict of Interest

The authors declare no conflict of interest.

## Keywords

conductivity, electron transport, framework materials, photoswitching, proton transport

Received: May 15, 2025
Revised: September 8, 2025
Published online:

[1] F. Hassan, Y. Tang, H. K. Bisoyi, Q. Li, *Adv. Mater.* **2024**, *36*, 2401912.
[2] A. Bakkar, F. Lafolet, D. Roldan, E. Puyoo, D. Jouvenot, G. Royal, E. Saint-Aman, S. Cobo, *Nanoscale* **2018**, *10*, 5436.
[3] M. Cao, Z. Cai, X. Chen, K. Yi, D. Wei, *J. Mater. Chem. C* **2017**, *5*, 9597.
[4] Y. Li, H. Zhang, C. Qi, X. Guo, *J. Mater. Chem.* **2012**, *22*, 4261.
[5] K. Xue, S. Hussain, S. Fan, X. Peng, *RSC Adv.* **2023**, *13*, 12646.
[6] Y. Chen, J. Qiu, X.-G. Zhang, H. Wang, W. Yao, Z. Li, Q. Xia, G. Zhu, J. Wang, *Chem. Sci.* **2022**, *13*, 5964.
[7] H.-Q. Liang, Y. Guo, Y. Shi, X. Peng, B. Liang, B. Chen, *Angew. Chem., Int. Ed.* **2020**, *59*, 7732.
[8] J. Keyvan Rad, Z. Balzade, A. R. Mahdavian, *J. Photochem. Photobiol., C* **2022**, *51*, 100487.
[9] F. Xiang, S. Chen, Z. Yuan, L. Li, Z. Fan, Z. Yao, C. Liu, S. Xiang, Z. Zhang, *JACS Au* **2022**, *2*, 1043.
[10] O. Burgos-Morales, M. Gueye, L. Lacombe, C. Nowak, R. Schmachtenberg, M. Hörner, C. Jerez-Longres, H. Mohsenin, H. J. Wagner, W. Weber, *Mater. Today Bio* **2021**, *11*, 100115.
[11] L. Hou, T. Leydecker, X. Zhang, W. Rekab, M. Herder, C. Cendra, S. Hecht, I. McCulloch, A. Salleo, E. Orgiu, P. Samorì, *J. Am. Chem. Soc.* **2020**, *142*, 11050.
[12] Y. Liu, M. Mostaghimi, A. Chandresh, S. Jana, W. Wenzel, L. Heinke, *Adv. Funct. Mater.* **2025**, https://doi.org/10.1002/adfm.202423539 .
[13] Y. Chen, B. Han, M. Gobbi, L. Hou, P. Samorì, *Adv. Mater.* **2025**, *37*, 2418281.
[14] J. Chen, W. Xu, *eScience* **2023**, *3*, 100178.
[15] S. V. Bachinin, A. Marunchenko, I. Matchenya, N. Zhestkij, V. Shirobokov, E. Gunina, A. Novikov, M. Timofeeva, S. A. Povarov, F. Li, V. A. Milichko, *Commun. Mater.* **2024**, *5*, 128.
[16] M. Kathan, S. Hecht, *Chem. Soc. Rev.* **2017**, *46*, 5536.
[17] Klán, P., J. Wirz, *Molecular Photoswitches: Chemistry, Properties, and Applications*, (Eds.: L. Zbigniew, Pianowski), Wiley-VCH, Weinheim, **2022**, pp. 4–18.
[18] J. Boelke, S. Hecht, *Adv. Opt. Mater.* **2019**, *7*, 1900404.
[19] J. Volarić, W. Szymanski, N. A. Simeth, B. L. Feringa, *Chem. Soc. Rev.* **2021**, *50*, 12377.
[20] C. García-Iriepa, M. Marazzi, L. M. Frutos, D. Sampedro, *RSC Adv.* **2013**, *3*, 6241.
[21] M. Irie, T. Fukaminato, K. Matsuda, S. Kobatake, *Chem. Rev.* **2014**, *114*, 12174.
[22] R. Berraud-Pache, E. Santamaría-Aranda, B. De Souza, G. Bistoni, F. Neese, D. Sampedro, R. Izsák, *Chem. Sci.* **2021**, *12*, 2916.

[23] S. L. Broman, M. B. Nielsen, *Phys. Chem. Chem. Phys.* **2014**, *16*, 21172.
[24] S. Molla, S. Bandyopadhyay, *J. Mater. Chem. C* **2024**, *12*, 17511.
[25] R. T. F. Jukes, J. Kühni, N. Salluce, P. Belser, L. De Cola, F. Hartl, *Dalton Trans.* **2009**, https://doi.org/10.1039/B821637C .
[26] S. Castellanos, F. Kapteijn, J. Gascon, *CrystEngComm* **2016**, *18*, 4006.
[27] M.-M. Russew, S. Hecht, *Adv. Mater.* **2010**, *22*, 3348.
[28] A. M. Rice, C. R. Martin, V. A. Galitskiy, A. A. Berseneva, G. A. Leith, N. B. Shustova, *Chem. Rev.* **2020**, *120*, 8790.
[29] Z. Wang, L. Heinke, J. Jelic, M. Cakici, M. Dommaschk, R. J. Maurer, H. Oberhofer, S. Grosjean, R. Herges, S. Bräse, K. Reuter, C. Wöll, *Phys. Chem. Chem. Phys.* **2015**, *17*, 14582.
[30] Y. Jiang, L. Heinke, *Langmuir* **2021**, *37*, 2.
[31] R. Haldar, L. Heinke, C. Wöll, *Adv. Mater.* **2020**, *32*, 1905227.
[32] G. A. Leith, C. R. Martin, A. Mathur, P. Kittikhunnatham, K. C. Park, N. B. Shustova, *Adv. Energy Mater.* **2022**, *12*, 2100441.
[33] A. Goulet-Hanssens, F. Eisenreich, S. Hecht, *Adv. Mater.* **2020**, *32*, 1905966.
[34] A. B. Grommet, L. M. Lee, R. Klajn, *Acc. Chem. Res.* **2020**, *53*, 2600.
[35] W. Danowski, T. Van Leeuwen, W. R. Browne, B. L. Feringa, *Nanoscale Adv.* **2021**, *3*, 24.
[36] M. Weiter, M. Vala, O. Zmeškal, S. Nešpůrek, P. Toman, *Macromol. Symp.* **2007**, *247*, 318.
[37] U. G. R. Lakmali, C. V. Hettiarachchi, *CrystEngComm* **2015**, *17*, 8607.
[38] D. Hermann, H. Emerich, R. Lepski, D. Schaniel, U. Ruschewitz, *Inorg. Chem.* **2013**, *52*, 2744.
[39] A. Modrow, D. Zargarani, R. Herges, N. Stock, *Dalton Trans.* **2011**, *40*, 4217.
[40] S. Bernt, M. Feyand, A. Modrow, J. Wack, J. Senker, N. Stock, *Eur. J. Inorg. Chem.* **2011**, *2011*, 5378.
[41] A. Modrow, D. Zargarani, R. Herges, N. Stock, *Dalton Trans.* **2012**, *41*, 8690.
[42] D. G. (Dan) Patel, I. M. Walton, J. M. Cox, C. J. Gleason, D. R. Butzer, J. B. Benedict, *Chem. Commun.* **2014**, *50*, 2653.
[43] K. Ohara, Y. Inokuma, M. Fujita, *Angew. Chem., Int. Ed.* **2010**, *49*, 5507.
[44] F. Zhang, X. Zou, W. Feng, X. Zhao, X. Jing, F. Sun, H. Ren, G. Zhu, *J. Mater. Chem.* **2012**, *22*, 25019.
[45] N. D. Shepherd, T. Wang, B. Ding, J. E. Beves, D. M. D'Alessandro, *Inorg. Chem.* **2021**, *60*, 11706.
[46] X. Yu, Z. Wang, M. Buchholz, N. Füllgrabe, S. Grosjean, F. Bebensee, S. Bräse, C. Wöll, L. Heinke, *Phys. Chem. Chem. Phys.* **2015**, *17*, 22721.
[47] A. Modrow, M. Feyand, D. Zargarani, R. Herges, N. Stock, *Z. Anorg. Allg. Chem.* **2012**, *638*, 2138.
[48] J. W. Brown, B. L. Henderson, M. D. Kiesz, A. C. Whalley, W. Morris, S. Grunder, H. Deng, H. Furukawa, J. I. Zink, J. F. Stoddart, O. M. Yaghi, *Chem. Sci.* **2013**, *4*, 2858.
[49] X. Meng, B. Gui, D. Yuan, M. Zeller, C. Wang, *Sci. Adv.* **2016**, *2*, 1600480.
[50] L. Heinke, M. Cakici, M. Dommaschk, S. Grosjean, R. Herges, S. Bräse, C. Wöll, *ACS Nano* **2014**, *8*, 1463.
[51] S. Castellanos, A. Goulet-Hanssens, F. Zhao, A. Dikhtiarenko, A. Pustovarenko, S. Hecht, J. Gascon, F. Kapteijn, D. Bléger, *Chem. Eur. J.* **2016**, *22*, 746.
[52] J. Park, D. Feng, S. Yuan, H.-C. Zhou, *Angew. Chem., Int. Ed.* **2015**, *54*, 430.
[53] S. Garg, H. Schwartz, M. Kozlowska, A. B. Kanj, K. Müller, W. Wenzel, U. Ruschewitz, L. Heinke, *Angew. Chem., Int. Ed. Eng.* **2019**, *58*, 1193.
[54] K. Müller, J. Helfferich, F. Zhao, R. Verma, A. B. Kanj, V. Meded, D. Bléger, W. Wenzel, L. Heinke, *Adv. Mater.* **2018**, *30*, 1706551.
[55] S. Mollick, J.-C. Tan, *Nat. Rev. Mater.* **2025**, *10*, 519.
[56] L. S. Xie, G. Skorupskii, M. Dincă, *Chem. Rev.* **2020**, *120*, 8536.
[57] R. A. Kharod, J. L. Andrews, M. Dincă, *Annu. Rev. Mater. Res.* **2022**, *52*, 103.
[58] J. J. Calvo, S. M. Angel, M. C. So, *APL Mater.* **2020**, *8*, 050901.
[59] R. Freund, S. Canossa, S. M. Cohen, W. Yan, H. Deng, V. Guillerm, M. Eddaoudi, D. G. Madden, D. Fairen-Jimenez, H. Lyu, L. K. Macreadie, Z. Ji, Y. Zhang, B. Wang, F. Haase, C. Wöll, O. Zaremba, J. Andreo, S. Wuttke, C. S. Diercks, *Angew. Chem., Int. Ed.* **2021**, *60*, 23946.
[60] Y.-H. Xiao, Z.-G. Gu, J. Zhang, *Nanoscale* **2020**, *12*, 12712.
[61] D. Blätte, F. Ortmann, T. Bein, *J. Am. Chem. Soc.* **2024**, *146*, 32161.
[62] A. Ciesielski, C. H. Hendon, K. A. Mirica, *J. Mater. Chem. C* **2024**, *12*, 6008.
[63] G. Gong, B. Yang, Y. Chen, N. Xia, Y. Xiong, D. A. Asamannaba, X. Chen, *Chem. Commun.* **2025**, *61*, 12885.
[64] B. Wang, Y. Liu, X. Chen, X.-T. Liu, Z. Liu, C. Lu, *Chem. Soc. Rev.* **2024**, *53*, 10189.
[65] R. Yuan, H. Sun, Z. Yan, H. He, *J. Solid State Chem.* **2021**, *297*, 122049.
[66] G. Gong, S. Lv, J. Han, F. Xie, Q. Li, N. Xia, W. Zeng, Y. Chen, L. Wang, J. Wang, S. Chen, *Angew. Chem., Int. Ed.* **2021**, *60*, 14831.
[67] H. Laeim, V. Molahalli, P. Prajongthat, A. Pattanaporkratana, G. Pathak, B. Phettong, N. Hongkarnjanakul, N. Chattham, *Polymers* **2025**, *17*, 130.
[68] R. Younas, F. Jubeen, N. Bano, S. Andreescu, H. Zhang, A. Hayat, *Biotechnol. Bioeng.* **2024**, *121*, 2017.
[69] X. Liu, M. Kozlowska, T. Okkali, D. Wagner, T. Higashino, G. Brenner-Weiß, S. M. Marschner, Z. Fu, Q. Zhang, H. Imahori, S. Bräse, W. Wenzel, C. Wöll, L. Heinke, *Angew. Chem., Int. Ed.* **2019**, *58*, 9590.
[70] R.-B. Lin, S. Xiang, W. Zhou, B. Chen, *Chem* **2020**, *6*, 337.
[71] S. K. Ramakrishna, K. Kundu, J. K. Bindra, S. A. Locicero, D. R. Talham, A. P. Reyes, R. Fu, N. S. Dalal, *J. Phys. Chem. C* **2021**, *125*, 3441.
[72] M. Mostaghimi, H. Pacheco Hernandez, Y. Jiang, W. Wenzel, L. Heinke, M. Kozlowska, *Commun. Chem.* **2023**, *6*, 275.
[73] G. C. Thaggard, J. Haimerl, K. C. Park, J. Lim, R. A. Fischer, B. K. P. Maldeni Kankanamalage, B. J. Yarbrough, G. R. Wilson, N. B. Shustova, *J. Am. Chem. Soc.* **2022**, *144*, 23249.
[74] Q. Huang, C. Wu, *Mater. Today Sustainability* **2022**, *18*, 100149.
[75] I. M. Walton, J. M. Cox, C. A. Benson, D. (Dan) G. Patel, Y.-S. Chen, J. B. Benedict, *New J. Chem.* **2016**, *40*, 101.
[76] Y. Jiang, Y. Liu, S. Grosjean, V. Bon, P. Hodapp, A. B. Kanj, S. Kaskel, S. Bräse, C. Wöll, L. Heinke, *Angew. Chem., Int. Ed.* **2023**, *62*, 202218052.
[77] F. Bigdeli, C. T. Lollar, A. Morsali, H.-C. Zhou, *Angew. Chem., Int. Ed.* **2020**, *59*, 4652.
[78] G. C. Thaggard, K. C. Park, J. Lim, B. K. P. Maldeni Kankanamalage, J. Haimerl, G. R. Wilson, M. K. McBride, K. L. Forrester, E. R. Adelson, V. S. Arnold, S. T. Wetthasinghe, V. A. Rassolov, M. D. Smith, D. Sosnin, I. Aprahamian, M. Karmakar, S. K. Bag, A. Thakur, M. Zhang, B. Z. Tang, J. A. Castaño, M. N. Chaur, M. M. Lerch, R. A. Fischer, J. Aizenberg, R. Herges, J.-M. Lehn, N. B. Shustova, *Nat. Commun.* **2023**, *14*, 7556.
[79] H. A. Schwartz, S. Olthof, D. Schaniel, K. Meerholz, U. Ruschewitz, *Inorg. Chem.* **2017**, *56*, 13100.
[80] N. Yanai, T. Uemura, M. Inoue, R. Matsuda, T. Fukushima, M. Tsujimoto, S. Isoda, S. Kitagawa, *J. Am. Chem. Soc.* **2012**, *134*, 4501.
[81] K. Healey, W. Liang, P. D. Southon, T. L. Church, D. M. D'Alessandro, *J. Mater. Chem. A* **2016**, *4*, 10816.
[82] B. Gui, Y. Meng, Y. Xie, K. Du, A. C.-H. Sue, C. Wang, *Macromol. Rapid Commun.* **2018**, *39*, 1700388.

[83] D. E. Williams, J. A. Rietman, J. M. Maier, R. Tan, A. B. Greytak, M. D. Smith, J. A. Krause, N. B. Shustova, *J. Am. Chem. Soc.* **2014**, *136*, 11886.
[84] S. Klokic, D. Naumenko, B. Marmiroli, F. Carraro, M. Linares-Moreau, S. D. Zilio, G. Birarda, R. Kargl, P. Falcaro, H. Amenitsch, *Chem. Sci.* **2022**, *13*, 11869.
[85] M. M. Sabzehmeidani, S. Gafari, S. Jamali, M. Kazemzad, *Appl. Mater. Today* **2024**, *38*, 102153.
[86] A. Gonzalez, M. Odaybat, M. Le, J. L. Greenfield, A. J. P. White, X. Li, M. J. Fuchter, G. G. D. Han, *J. Am. Chem. Soc.* **2022**, *144*, 19430.
[87] A. Ahamed, C. Bartolo-Perez, A. S. Mayet, S. Ghandiparsi, G. Ariño-Estrada, X. Zhou, J. Bec, S.-Y. Wang, L. Marcu, S. Islam, *Quantum Sensing and Nano Electronics and Photonics XVIII* (Eds.: M. Razeghi, G. A. Khodaparast, M. S. Vitiello), SPIE, San Francisco, United States, **2022**, p. 25.
[88] I. K. Januariyasa, F. Borbone, M. Salvatore, S. L. Oscurato, *ACS Appl. Mater. Interfaces* **2023**, *15*, 43183.
[89] J.-S. M. Lee, H. Sato, *Nat. Chem.* **2020**, *12*, 584.
[90] A. B. Kanj, K. Müller, L. Heinke, *Macromol. Rapid Commun.* **2018**, *39*, 1700239.
[91] W.-Q. Fu, M. Liu, Z.-G. Gu, S.-M. Chen, J. Zhang, *Cryst. Growth Des.* **2016**, *16*, 5487.
[92] B. Liu, O. Shekhah, H. K. Arslan, J. Liu, C. Wöll, R. A. Fischer, *Angew. Chem., Int. Ed.* **2012**, *51*, 807.
[93] Z. Wang, K. Müller, M. Valášek, S. Grosjean, S. Bräse, C. Wöll, M. Mayor, L. Heinke, *J. Phys. Chem. C* **2018**, *122*, 19044.
[94] A. B. Kanj, A. Chandresh, A. Gerwien, S. Grosjean, S. Bräse, Y. Wang, H. Dube, L. Heinke, *Chem. Sci.* **2020**, *11*, 1404.
[95] S. Klokic, B. Marmiroli, D. Naumenko, G. Birarda, S. Dal Zilio, M. D. J. Velásquez-Hernández, P. Falcaro, L. Vaccari, H. Amenitsch, *CrystEngComm* **2024**, *26*, 2228.
[96] S. Kouser, A. Hezam, M. J. N. Khadri, S. A. Khanum, *J. Porous Mater.* **2022**, *29*, 663.
[97] Z. Zheng, Z. Rong, H. L. Nguyen, O. M. Yaghi, *Inorg. Chem.* **2023**, *62*, 20861.
[98] R. Wang, H. Lyu, G. S. H. Poon Ho, H. Chen, Y. Yuan, K. Bang, Y. Kim, *Small* **2024**, *20*, 2306634.
[99] K. Geng, T. He, R. Liu, S. Dalapati, K. T. Tan, Z. Li, S. Tao, Y. Gong, Q. Jiang, D. Jiang, *Chem. Rev.* **2020**, *120*, 8814.
[100] M. Souto, D. F. Perepichka, *J. Mater. Chem. C* **2021**, *9*, 10668.
[101] Y. Zhu, S. Jiang, X. Jing, X. Feng, *Trends Chem.* **2022**, *4*, 128.
[102] Y. Zhao, Y. Han, Y. Yu, *Chem. Eng. J.* **2024**, *497*, 154997.
[103] G. A. Leith, A. M. Rice, B. J. Yarbrough, A. A. Berseneva, R. T. Ly, C. N. Buck, D. Chusov, A. J. Brandt, D. A. Chen, B. W. Lamm, M. Stefik, K. S. Stephenson, M. D. Smith, A. K. Vannucci, P. J. Pellechia, S. Garashchuk, N. B. Shustova, *Angew. Chem., Int. Ed.* **2020**, *59*, 6000.
[104] Y. Yang, A. P. Sandra, A. Idström, C. Schäfer, M. Andersson, L. Evenäs, K. Börjesson, *J. Am. Chem. Soc.* **2022**, *144*, 16093.
[105] F. Yu, W. Liu, B. Li, D. Tian, J. Zuo, Q. Zhang, *Angew. Chem., Int. Ed.* **2019**, *58*, 16101.
[106] G. Das, T. Prakasam, M. A. Addicoat, S. K. Sharma, F. Ravaux, R. Mathew, M. Baias, R. Jagannathan, M. A. Olson, A. Trabolsi, *J. Am. Chem. Soc.* **2019**, *141*, 19078.
[107] P. Li, M. R. Ryder, J. F. Stoddart, *Acc. Mater. Res.* **2020**, *1*, 77.
[108] R. Liang, J. Samanta, B. Shao, M. Zhang, R. J. Staples, A. D. Chen, M. Tang, Y. Wu, I. Aprahamian, C. Ke, *Angew. Chem., Int. Ed.* **2021**, *60*, 23176.
[109] Y. Gao, Y. Yang, Y. Wei, Y. Li, H. Cai, C. Wu, *Adv. Funct. Mater.* **2025**, *35*, 2416025.
[110] X. Liu, Y. Ye, X. He, Q. Niu, Z. Li, *Angew. Chem., Int. Ed.* **2025**, *64*, 202508976.
[111] P. K. Kundu, G. L. Olsen, V. Kiss, R. Klajn, *Nat. Commun.* **2014**, *5*, 3588.
[112] W. Danowski, T. Van Leeuwen, S. Abdolahzadeh, D. Roke, W. R. Browne, S. J. Wezenberg, B. L. Feringa, *Nat. Nanotechnol.* **2019**, *14*, 488.
[113] Y. Jiang, W. Danowski, B. L. Feringa, L. Heinke, *Angew. Chem., Int. Ed.* **2023**, *62*, 202214202.
[114] J. Sheng, J. Perego, S. Bracco, W. Czepa, W. Danowski, S. Krause, P. Sozzani, A. Ciesielski, A. Comotti, B. L. Feringa, *Adv. Mater.* **2024**, *36*, 2305783.
[115] E. Jin, V. Bon, S. Das, A. D. D. Wonanke, M. Etter, M. A. Karlsen, A. De, N. Bönisch, T. Heine, S. Kaskel, *J. Am. Chem. Soc.* **2025**, *147*, 8568.
[116] D. K. Maity, A. Dey, S. Ghosh, A. Halder, P. P. Ray, D. Ghoshal, *Inorg. Chem.* **2018**, *57*, 251.
[117] E. A. Dolgopolova, V. A. Galitskiy, C. R. Martin, H. N. Gregory, B. J. Yarbrough, A. M. Rice, A. A. Berseneva, O. A. Ejegbavwo, K. S. Stephenson, P. Kittikhunnatham, S. G. Karakalos, M. D. Smith, A. B. Greytak, S. Garashchuk, N. B. Shustova, *J. Am. Chem. Soc.* **2019**, *141*, 5350.
[118] H.-Q. Liang, Y. Guo, X. Peng, B. Chen, *J. Mater. Chem. A* **2020**, *8*, 11399.
[119] Z.-Y. Liu, H. Zhang, X.-Y. Ren, H.-B. Luo, J. Zhang, X.-M. Ren, *ACS Mater. Lett.* **2024**, *6*, 461.
[120] Y. Li, A. Chandresh, H. Lin, N. Vankova, D. Mutruc, T. Heine, S. Hecht, L. Heinke, *Adv. Mater.* **2025**, *37*, 2419195.
[121] D.-W. Lim, H. Kitagawa, *Chem. Rev.* **2020**, *120*, 8416.
[122] S. Fratini, D. Mayou, S. Ciuchi, *Adv. Funct. Mater.* **2016**, *26*, 2292.
[123] S. Giannini, J. Blumberger, *Acc. Chem. Res.* **2022**, *55*, 819.
[124] R. Haldar, M. Kozlowska, M. Ganschow, S. Ghosh, M. Jakoby, H. Chen, F. Ghalami, W. Xie, S. Heidrich, Y. Tsutsui, J. Freudenberg, S. Seki, I. A. Howard, B. S. Richards, U. H. F. Bunz, M. Elstner, W. Wenzel, C. Wöll, *Chem. Sci.* **2021**, *12*, 4477.
[125] K. Kreuer, A. Rabenau, W. Weppner, *Angew. Chem., Int. Ed. Eng.* **1982**, *21*, 208.
[126] X. Chen, K. Takahashi, K. Kokado, T. Nakamura, I. Hisaki, *Mater. Adv.* **2021**, *2*, 5639.
[127] P. Ramaswamy, N. E. Wong, G. K. H. Shimizu, *Chem. Soc. Rev.* **2014**, *43*, 5913.
[128] P. Atkins, J. de Paula, *ATKINS' PHYSICAL CHEMISTRY*, 8th ed., Oxford University Press, Oxford England, **2006**.
[129] L. Zhu, H. Yang, T. Xu, F. Shen, C. Si, *Nano-Micro Lett.* **2025**, *17*, 87.
[130] D. Moldenhauer, F. Gröhn, *Chem. Eur. J.* **2017**, *23*, 3966.
[131] H. Gao, T. Guo, Y. Chen, Y. Kong, Z. Peng, *J. Mol. Struct.* **2016**, *1123*, 426.
[132] S. Fu, E. Jin, H. Hanayama, W. Zheng, H. Zhang, L. Di Virgilio, M. A. Addicoat, M. Mezger, A. Narita, M. Bonn, K. Müllen, H. I. Wang, *J. Am. Chem. Soc.* **2022**, *144*, 7489.
[133] S. Ghosh, Y. Tsutsui, T. Kawaguchi, W. Matsuda, S. Nagano, K. Suzuki, H. Kaji, S. Seki, *Chem. Mater.* **2022**, *34*, 736.
[134] R. Dong, P. Han, H. Arora, M. Ballabio, M. Karakus, Z. Zhang, C. Shekhar, P. Adler, P. S. Petkov, A. Erbe, S. C. B. Mannsfeld, C. Felser, T. Heine, M. Bonn, X. Feng, E. Cánovas, *Nat. Mater.* **2018**, *17*, 1027.
[135] C. Scheiger, J. F. Pöhls, M. Mostaghimi, L. Pilz, M. Kozlowska, Y. Liu, L. Heinke, C. C. B. Bufon, R. T. Weitz, W. Wenzel, C. Wöll, *Mater. Horiz.* **2025**, *12*, 6189.
[136] V. Coropceanu, J. Cornil, D. A. Da Silva Filho, Y. Olivier, R. Silbey, J.-L. Brédas, *Chem. Rev.* **2007**, *107*, 926.
[137] G. Y. Zhu, Y. Qin, M. Meng, S. Mallick, H. Gao, X. Chen, T. Cheng, Y. N. Tan, X. Xiao, M. J. Han, M. F. Sun, C. Y. Liu, *Nat. Commun.* **2021**, *12*, 456.

[138] R. Dessauer, *Photochemistry, History and Commercial Applications of Hexaarylbiimidazoles*, Ed., R. Dessauer, Elsevier, Science B.V., Amsterdam, **2006**, pp. 21–26.
[139] Y. Liu, Y. Jiang, L. Heinke, *Langmuir* **2024**, *40*, 474.
[140] P. Qin, S. Okur, C. Li, A. Chandresh, D. Mutruc, S. Hecht, L. Heinke, *Chem. Sci.* **2021**, *12*, 15700.
[141] K.-D. Kreuer, *Chem. Mater.* **1996**, *8*, 610.
[142] C. Qian, R. Wang, F. Yu, H. Liu, C. Guo, K. Sun, J. Li, W. Bao, *Crystals* **2022**, *12*, 1405.
[143] R. K. Parashar, P. Jash, M. Zharnikov, P. C. Mondal, *Angew. Chem., Int. Ed.* **2024**, *63*, 202317413.
[144] Y. He, S. Yang, Y. Fu, F. Wang, J. Ma, G. Wang, G. Chen, M. Wang, R. Dong, P. Zhang, X. Feng, *Small Struct.* **2021**, *2*, 2000095.
[145] S. Gao, Y. Ren, D. Zhang, X. Wu, Y. Xie, L. Sun, R. Li, F. Yang, W. Hu, *J. Mater. Chem. C* **2024**, *12*, 6943.
[146] Y. Luo, S. Bag, O. Zaremba, A. Cierpka, J. Andreo, S. Wuttke, P. Friederich, M. Tsotsalas, *Angew. Chem., Int. Ed. Eng.* **2022**, *61*, 202200242.
[147] G. Tom, S. P. Schmid, S. G. Baird, Y. Cao, K. Darvish, H. Hao, S. Lo, S. Pablo-García, E. M. Rajaonson, M. Skreta, N. Yoshikawa, S. Corapi, G. D. Akkoc, F. Strieth-Kalthoff, M. Seifrid, A. Aspuru-Guzik, *Chem. Rev.* **2024**, *124*, 9633.

**Helmy Pacheco Hernandez** was born in Veracruz, Mexico. She graduated in 2018 with a degree in Chemical Engineering from the Instituto Tecnológico de Veracruz and obtained her M.Sc. in Materials Engineering from Universidad Autónoma Metropolitana (UAM) Azcapotzalco, Mexico City, in 2021. She is currently a Ph.D. candidate in Chemistry at the Karlsruhe Institute of Technology in the Multiscale Materials Modelling and Virtual Design group at the Institute of Nanotechnology. Her research centers on the properties of porous framework materials, especially on computational studies of the electronic and optical properties of MOFs.

**Stefan Hecht** studied chemistry at Humboldt University and UC Berkeley, where he carried out his doctoral research with Jean Fréchet. He started his independent career at Free University Berlin and subsequently at the MPI for Coal Research in Mülheim/Ruhr before accepting a call to Humboldt University as full professor in 2006. From 2019 until 2022 he was Scientific Director of the DWI Leibniz Institute for Interactive Materials and held the Chair of Macromolecular Chemistry at RWTH Aachen University before returning to his alma mater as Einstein Professor and Founding Director of the Center for the Science of Materials Berlin.

**Wolfgang Wenzel** studied physics at Ohio State University, where he received his M.S. (1988) and Ph.D. (1990). After a postdoctoral stay with Nobel Laureate K.G. Wilson, he became assistant professor at the University of Dortmund, completing his habilitation in 1997. In 2001, he joined the Karlsruhe Institute of Technology as head of the Nanoscale and Biomolecular Simulation group. He is currently a professor in the physics department and department head at the Institute of Nanotechnology. His research focuses on computational materials science, nanotechnology, and biomolecular simulations.

**Lars Heinke** studied physics in Greifswald and Leipzig and earned his Ph.D. from Leipzig University in 2009. Following postdoctoral stays at the Fritz-Haber Institute in Berlin and at the Lawrence Berkeley National Laboratory in California, his independent research started at the Karlsruhe Institute of Technology. Since 2024, he is a full professor for physical chemistry at the Freie Universitôt Berlin. His research focuses on functional nanoporous films, studying their physicochemical properties with particular emphasis on diffusion, conduction and nanoconfinement effects as well as the development of photoresponsive smart coatings.

**Mariana Kozlowska** completed her Ph.D. in chemistry in Poland (2017) and moved to Germany as a research fellow at the Technical University of Berlin (Maria Andrea Mroginski). In 2018, she joined the Karlsruhe Institute of Technology (KIT) to work with Wolfgang Wenzel on multiscale simulations of soft matter materials. Since 2024, she has been a KIT Associate Fellow and the Head of the DNA Unit of the Virtual Materials Design platform at KIT. Her research combines first-principles and scale-bridging simulations to link molecular structure with material properties by elucidating photophysical behavior, intermolecular interactions, and assembly processes in functional materials.